

FMH606 Master's Thesis 2018
Electrical Power Engineering

Power loss measurements in MV switchgear for Cigré-working group

Sandra Helland

Course: FMH606 Master's Thesis, 2018

Title: Power loss measurements in MV switchgear for Cigré-working group

Number of pages: 96

Keywords: Power loss, Temperature measurements, Bulk resistance, Contact resistance, Switchgear, Knife switch

Student: Sandra Helland

Supervisor: Elin Fjeld / Wilhelm Rondeel

External partner: ABB AS

Availability: Open

Summary:

Working group A3.36 from Cigré is studying to what degree simulations can be used to predict the steady state temperature of MV and HV switchgear. The result of this thesis will be provided to the working group. The aim of the thesis is to assemble a realistic test device, which has a realistic design, power input and number of contacts/connections. The test device consists of a three-phase setup with knife switches inside an enclosure without ventilation.

Tests have been performed on the test device to find the bulk and contact resistance and compared the bulk resistance to the theoretical value, the power loss is estimated, and the steady state temperature is found. Two temperature rise tests have been performed, one with magnetic bolts and washers in the bushings and one with nonmagnetic bolts and washers.

It was found large variations in the contact resistances of the rotating contacts of the knife switches, the steady state temperatures of the current path were found to be higher than the temperatures of similar switchgears, even though the power loss of the test device is less than the power loss in the similar switchgear. The magnetic bolts had an impact of the heat generation of the conductors, when the bolts were replaced with nonmagnetic bolts the steady state temperature decreased and the power loss stayed approximately the same. The IEC temperature limits were exceeded by great extent in both tests. Overall, the temperature of the current path should be reduced for the test device to be more realistic.

The University College of Southeast Norway takes no responsibility for the results and conclusions in this student report.

Preface

This report is a result of the master's thesis "Power loss measurements in MV switchgear for Cigré-working group". The report is written during the final semester of the master degree Electrical Power Engineering at USN.

I would like to thank the supervisors Elin Fjeld and Wilhelm Rondeel for the valuable guidance during the semester.

Porsgrunn, 15.05.2018

Sandra Helland

Contents

1	Introduction.....	13
1.1	Background of the thesis	13
1.2	Purpose of the thesis.....	14
1.3	Objectives	14
1.4	Outline of the report	15
2	Theory	17
2.1	Electrical resistance	17
2.1.1	Contact resistance	17
2.1.2	Bulk resistance	18
2.2	Power loss and heat generation	19
2.3	IEC temperature limits.....	20
2.4	IEC model for estimating the air temperature inside enclosure	21
3	System description.....	23
3.1	Overview.....	23
3.1.1	RMU enclosure	23
3.1.2	Small enclosure	25
3.2	Switches.....	25
3.3	Conductors	27
4	Performance of the experiments	29
4.1	Equipment for measuring.....	29
4.1.1	Thermocouples and logging device	29
4.1.2	Mounting of the thermocouples	32
4.1.3	Additional thermocouples for test 2 with nonmagnetic bolts	34
4.2	Procedure for installing the setup	35
4.3	Resistance and power loss measurements	36
4.3.1	Bulk resistance of the switch.....	36
4.3.2	Contact resistances of the switch.....	36
4.3.3	Total resistance of the current path inside RMU enclosure.....	36
4.3.4	Total resistance during steady state temperature	36
4.3.5	Power loss	37
4.4	Temperature rise measurements.....	37
4.4.1	Steady state temperatures test 1: magnetic bolts	37
4.4.2	Steady state temperatures test 2: nonmagnetic bolts.....	37
4.4.3	Temperatures requested by the working group	38
5	Resistance and power loss	39
5.1	Bulk resistance results	39
5.1.1	Theoretical bulk resistance of the knife switch and replacement bar	39
5.1.2	Theoretical bulk resistance of the conductors	40
5.1.3	Measured bulk resistance of the switch	41
5.2	Contact resistance results	42
5.2.1	Measured contact resistances of the switch placed in the small enclosure	42
5.2.2	Contact resistances of the current path placed in the RMU enclosure	43
5.3	Total resistance results.....	44
5.3.1	Total theoretical bulk resistance of the current path	44

Contents

5.3.2	Measured total resistance of the current path inside RMU enclosure	45
5.4	Resistance during steady state temperature results	46
5.4.1	Estimated increase in resistance with temperature rise	46
5.4.2	Measured resistance at steady state temperature	47
5.5	Power loss estimate	47
5.6	Discussions	48
5.6.1	Bulk resistance	48
5.6.2	Contact resistance	48
5.6.3	Total resistance and power loss	49
5.6.4	Resistance during steady state temperature	51
6	Temperature rise	53
6.1	Estimate of air temperature inside RMU enclosure	53
6.2	Air temperature inside the enclosure	55
6.2.1	Measured steady state air temperature rise for test 1: magnetic bolts	55
6.2.2	Measured steady state air temperature rise for test 2: nonmagnetic bolts	56
6.2.3	Comparison of the steady state air temperature result of test 1 and test 2	56
6.3	Steady state temperature of the current path	57
6.3.1	Measured steady state temperature of test 1: magnetic bolts	57
6.3.2	Measured steady state temperature of test 2: nonmagnetic bolts	58
6.4	Influence of magnetic bolts and washers	61
6.4.1	Air inside RMU enclosure	61
6.4.2	Conductors and switches	62
6.5	Influence of mounting mechanisms of the thermocouples	63
6.6	Discussions	64
6.6.1	IEC temperature limits	64
6.6.2	Steady state air temperature of the RMU enclosure	64
6.6.3	Steady state temperature of the current path	65
7	Heat transfer coefficient	69
7.1	Calculation of the heat transfer coefficient	69
7.2	Discussion	71
8	Conclusion	73

Nomenclature

Symbol:	Definition:
AC	Alternating current
Ag	Silver
After heating	The switchgear at reference temperature after heating up the switchgear to steady state temperature
Before heating	The switchgear at reference temperature before the switchgear is heater up to steady state temperature
CB	Circuit breaker
Cigré	International Council on Large Electric Systems
Cu	Copper
“Cold resistance”	Resistance during reference temperature
DC	Direct current
HV	High Voltage (above 35kV)
IEC	International Electrotechnical Commission
LBS	Load break switch
LV	Low voltage (up to 1kV)
MV	Medium Voltage (between 1kV and 35kV)
Ni	Nickel
Reference temperature	Room temperature, approximately 20°C
RMU	Ring Main Unit
Steady state temperature	Temperature increase less than 1°C per hour [1]
USN	University of Southeast Norway
“Warm resistance”	Resistance during steady state temperature

Symbols

Symbol:	Unit:	Definition:
A	$[\text{mm}^2]$	Cross-sectional area of conductor
c	$[-]$	Temperature distribution factor
C	$[\text{J}/\text{kg} * ^\circ\text{C}]$	Specific heat
d	$[-]$	Temperature rise factor for internal horizontal partitions
h	$[\text{W}/\text{m}^2 * ^\circ\text{C}]$	Heat transfer coefficient
I	$[\text{A}]$	Current
k	$[-]$	Enclosure constant
l	$[\text{m}]$	Length of conductor
P	$[\text{W}]$	Active power
R	$[\Omega]$	Electrical resistance
T	$[\text{C}]$	Temperature
U	$[\text{m}^2]$	Surface area
V	$[\text{V}]$	Voltage
V_L	$[\text{m}^3]$	Volume of conductor
x	$[-]$	Exponent
α	$[\text{K}^{-1}]$	Temperature coefficient
γ	$[\text{kg}/\text{m}^3]$	Density
ΔT	$[\text{C}]$	Temperature difference
ϑ	$[\text{C}]$	Given temperature
ρ	$[\text{mm}^2\Omega/\text{m}]$	Specific resistance

1 Introduction

In this chapter, an introduction to the thesis will be given.

1.1 Background of the thesis

The power system is a complex system where large amounts of power are transferred over long distances at different voltage levels. Figure 1.1 shows a simplified drawing of the power system.

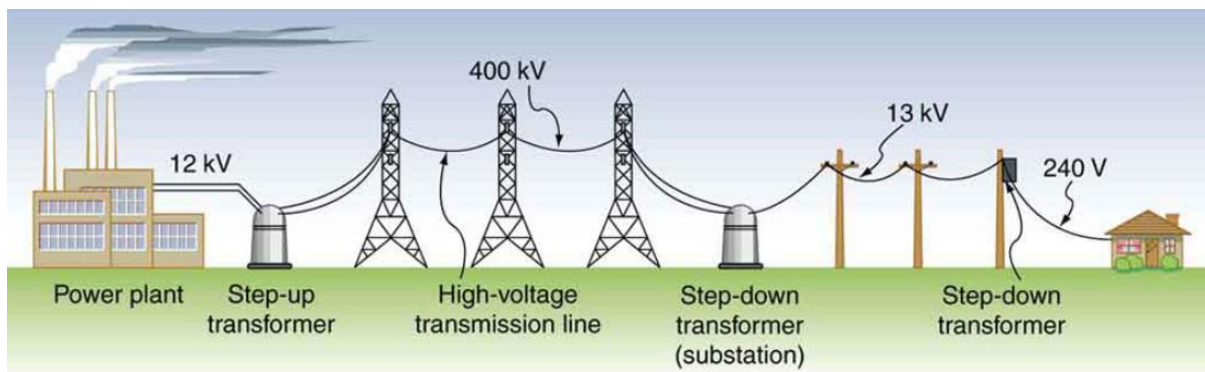


Figure 1.1 – Overview of the power system [2]

The ability to control the system is important to secure a reliable system. Controlling the system involves de-energizing parts of the system for regular maintenance and automatic shutdown to avoid damages. For this purpose, protective system is designed. Switchgear is a part of the protective system and is a general term for components designed to operate the making and breaking of the power supply. There are several types of switchgear used for different purposes, load break switches (LBS) are designed to operate under normal conditions and circuit breakers (CB) are designed to operate for faults [2]. Figure 1.2 shows two examples of how switchgear could look like.



MV indoor switchgear [4]



HV outdoor switchgear [5]

Figure 1.2 – Pictures of examples of switchgear types

1.2 Purpose of the thesis

Switchgear is exposed to electrical and mechanical stress. Stress is a mechanism that reduces the lifetime of the switchgear. Typical stress factors are abnormal environment or abnormal operating conditions. Temperature is a concern when talking about operating conditions. The higher the temperature, the accelerated aging are expected.

For all switchgear, a type test is executed. The type test shall provide the necessary characteristics of the switchgear, and includes measurements of resistance of the main circuit, mechanical tests, making and breaking tests and temperature rise test [2].

The temperature rise test demands from the IEC standard 62271-1 are given by very strict guidelines and requires relatively large resources of the manufacturer to execute. It is beneficial to have easier methods to predict and verify the temperature rise of switchgear. Such a method could benefit when dealing with the early stages of designing switchgear.

Cigré (International Council on Large Electric Systems) is an association where experts from all around the world work together in working groups to improve electric power systems. Simulation technologies have an increasing role in the development and verification of the performance of equipment, and the working group A3.36 is studying to what degree simulations can be used to predict the steady state temperature rise of MV and HV switchgear. The result of this thesis will be compared with the simulation results of the respective companies involved in the working group.

1.3 Objectives

The aim of the thesis is to assemble a realistic test device. The test device should have a design that is close to a real switchgear. The test device should consist of three phases. The resistance of the path should be within reasonable limits to get a proper power loss and temperature rise. The results found by measuring and tests should be compared to relevant results from similar experiments.

To fulfill this aim, the following objectives are performed:

- The switchgear is to be assembled to a test device.
- Calculate theoretical bulk resistance.
- Measure bulk and contact resistance.
- Estimate and measure resistance during full load conditions.
- Measure the temperature rise at full load conditions.
- Compare the steady state temperature with relevant IEC limits
- Estimate and measure total power loss during full load conditions
- Investigate the influence of magnetic bolts in the bushing-connection
- Calculate the heat transfer coefficient

The problem description is given in Appendix A.

1.4 Outline of the report

This report consists of 8 chapters, including chapter 1: Introduction.

Chapter 1: Introduction

Chapter 1 presents the background information and purpose of the thesis.

Chapter 2: Theory

Chapter 2 presents some of the relevant theory used in the report.

Chapter 3: System description

Chapter 3 contain a description of the test device and presents relevant data of the components.

Chapter 4: Performance of experiments

Chapter 4 contains the description of the performance of the experiments, the procedure for installing the setup and the equipment that is used.

Chapter 5: Resistance and power loss

Chapter 5 presents the results and the discussion of the resistance and power loss measurements.

Chapter 6: Temperature rise

Chapter 6 presents the results and the discussion of the temperature rise measurements.

Chapter 7: Calculation of the heat transfer coefficient

Chapter 7 contains the calculation of the heat transfer coefficient.

Chapter 8: Conclusion

Chapter 8 contains a final conclusion to the results found in the report.

2 Theory

In this chapter, some of the theory used through the report will be presented.

2.1 Electrical resistance

The electric resistance of an electric switch consists of two attributes. The resistance of the material in the conductive parts and the resistance occurring when two separately conductive parts are pressed together.

The resistance of the material is referred to as the bulk resistance. The resistance of the connection of two individual parts is referred to as contact resistance. Figure 2.1 shows an illustration of where the bulk and contact resistance appear on an electrical switch.

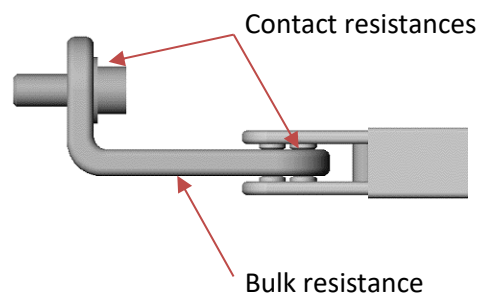


Figure 2.1 – Illustration where the bulk and contact resistance appear on an electrical switch

The total resistance of a switch is the sum of the bulk resistance and the contact resistance, as shown in Equation (2.1).

$$R_{Switch} = R_{Bulk-Switch} + R_{Contact-Switch} \quad (2.1)$$

2.1.1 Contact resistance

An electrical contact allows a current to pass between two separately conductive parts. Electrical contacts are essential for making and breaking in the power system and different types of contacts are used for different purposes. Figure 2.2 shows an example of a bolted contact.

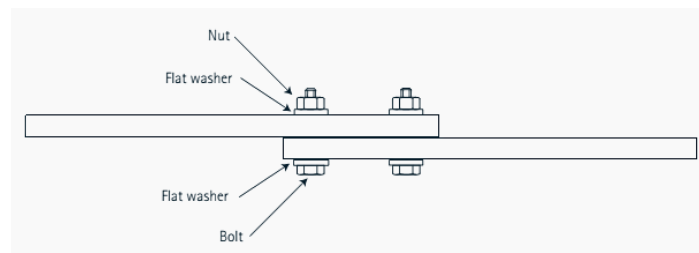


Figure 2.2 – Example of bolted contact [3]

The size of the resistance is dependent on the surface structure of the material and contact pressure [5]. The surface of the material will never be perfectly even, and there will occur certain spots where the contact members are in contact with each other. These spots of contact are referred to as a-spots, and the size and amount of these spots will determine the contact resistance [1].

The number of a-spots can be manipulated in some cases, examples of such cases could be cleaning the surface or create a greater contact pressure. Because of the a-spots, the contact resistance will be different for every contact.

The contact resistance is difficult to calculate theoretically because of the a-spots and is often found by measuring or by using historical data to estimate a value.

2.1.2 Bulk resistance

The bulk resistance is strictly dependent on the properties of the conductor, such as the length, cross-section and the properties of the material itself. Equation (2.2) shows the expression used to calculate the bulk resistance. The specific resistance is different for different types of materials and will change if conditions such as temperature changes.

$$R_{Bulk} = \frac{l * \rho}{A} \quad (2.2)$$

R_{Bulk} = Bulk resistance [Ω]

ρ = Specific resistance [$\Omega * \text{mm}^2/\text{m}$]

l = Length of conductor [m]

A = Cross section of the conductor [mm^2]

The specific resistance of some materials is given in Table 2.1 at reference temperature. The parameters for hard copper is used during this report, marked with bold font in Table 2.1.

Table 2.1 – Specific resistance for some materials [8]

Material	Specific electric resistance ρ_0 [$\text{mm}^2\Omega/\text{m}$]	Temperature coefficient α [$1/^\circ\text{C}$]
Aluminum, 99,5% Al, soft	0,0278	$4,0 * 10^{-3}$
Copper, soft	0,01754	$4,0 * 10^{-3}$
Copper, hard*	0,01786	$3,92 * 10^{-3}$

**parameter used throughout this report*

Theory

The specific resistance is dependent on the temperature of the conductor, and if the temperature differs from the reference temperature, the specific resistance is increases. Equation (2.3) shows the formula to calculate the specific resistance at a given temperature.

$$\rho_{\theta} = \rho_0[1 + \alpha * \Delta T] \quad (2.3)$$

ρ_{θ} = Specific resistance at given temperature [$\Omega * \text{mm}^2/\text{m}$]

ρ_0 = Specific resistance at reference temperature [$\Omega * \text{mm}^2/\text{m}$]

α = Temperature coefficient [$1/^{\circ}\text{C}$]

ΔT = Temperature change [$^{\circ}\text{C}$]

2.2 Power loss and heat generation

The current flowing and the resistance of the conductors will result in a power loss in the switchgear. Contributions from iron losses and skin effect are considered small in this case and is neglected [6].

Equation (2.4) shows the formula to calculate the power loss.

$$P_{loss} = R_{total} * I^2 \quad (2.4)$$

P_{loss} = Power loss [W]

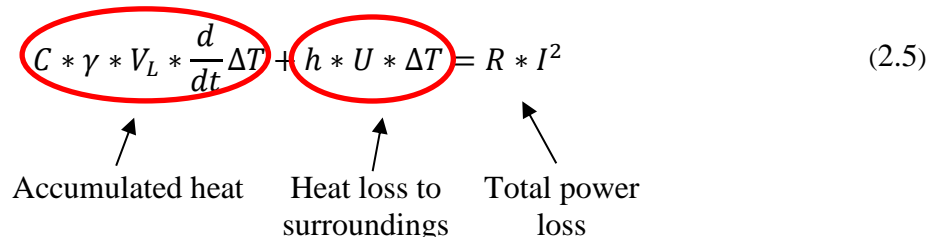
I = Current [A]

R_{Total} = Total resistance of the current path [Ω]

The power loss in the conductors and switches causes the temperature to increase when the switchgear is connected to a power source. Immediately after a current of significantly magnitude is applied to the switchgear, the temperature of the conductors starts to increase.

The temperature of the conductors will increase until steady state temperature is reached. Steady state temperature is defined as a change in temperature less than 1°C per hour. The temperature of the surroundings will increase gradually as the temperature of the conductors increases, due to heat transfer. Equation (2.5) explain the relationship between the generated heat in the conductors and the heat transfer to the surroundings.

$$C * \gamma * V_L * \frac{d}{dt} \Delta T + h * U * \Delta T = R * I^2 \quad (2.5)$$



C = Specific heat [J/kg * °C]

γ = Density [kg/m³]

V_L = Volume of conductor [m³]

ΔT = Temperature difference between conductor and air [°C]

h = Heat transfer coefficient [W/m² * °C]

U = Surface area [m²]

The first term in Equation (2.5) is the power needed to heat up the conductors. The second term in Equation (2.5) is the power lost to the surroundings. When the temperature of the conductors and surroundings are close to reference temperature, the heat transfer coefficient is very low and the amount of heat transferred to the surroundings is therefore low. Gradually as the temperature of the conductors increases, the heat transfer coefficient increases and the power loss to the surroundings increases. After some time, the heat loss to the surroundings will be equal to the total power loss and the temperatures of the conductors has reached a maximum temperature.

2.3 IEC temperature limits

IEC has set some limits for the temperature rise and the steady state temperature of conductors. These limits are shown in Table 2.2. There are three limits that's relevant in this report, marked with bold font in Table 2.2.

Table 2.2 – IEC temperature limits [6]

IEC –Maximum temperatures for electrical contacts		
	Maximum temperature (maximum ambient 40°C) [°C]	Maximum temperature rise (maximum ambient 40°C) [°C]
Spring loaded contacts		
Bare copper or copper alloy	75	35
Silver or nickel plated	105	65
Bolted connections		
Bare copper, bare copper alloy or aluminum alloy	90	50
Silver or nickel plated	115	75

Theory

The main purpose of the limits in Table 2.2 is to maintain the lifetime of the switchgear. Exceeding these temperature limits causes accelerated degradation of the contact surfaces and could over time lead to complete failure of the equipment. The switchgear should though be able to have a short-time overload capability [6].

2.4 IEC model for estimating the air temperature inside enclosure

The air temperature inside an enclosure could be estimated using the method described in the technical report IEC TR-60890. The report gives an empirical method to estimate the temperature rise of the air inside an enclosure for several types of switchgear modules [10].

The method given in the report describes the approach to calculate two temperatures of interest in this report, the middle air temperature of the enclosure and the top air temperature of the enclosure. Equation (2.6-2.7) shows the formulas needed to estimate the temperatures.

$$\Delta t_{0,5} = k * d * P_{loss}^x \quad (2.6)$$

$\Delta t_{0,5}$ = Temperature rise of air at mid-height of enclosure [°C]

k = Enclosure constant

d = Temperature rise factor for internal horizontal partitions inside enclosure

x = Exponent

$$\Delta t_{1,0} = c * \Delta t_{0,5} \quad (2.7)$$

$\Delta t_{1,0}$ = Temperature rise of air at top of enclosure [°C]

c = Temperature distribution factor

The variables in Equation (2.6-2.7) is based on a corrected surface area of the enclosure. The surface area is multiplied with a surface correction factor, b . The surface factor is defined for different types of surface, Table 2.3 shows the factors for the surfaces needed to estimate the air temperature rise.

Table 2.3 – Definitions and surface factor for some surfaces

Defined surface	Surface factor b
Exposed top	1,4
Exposed side	0,9
Covered side	0,5
Floor	0

3 System description

In this chapter, a description of the test device and the components used to conduct the experiments will be given.

3.1 Overview

Two enclosures are used for conducting the experiments. One for performing temperature rise tests and one for performing resistance measurements. The two next subchapters gives a short description of both.

3.1.1 RMU enclosure

The RMU enclosure forms the closed enclosure of the test device. The RMU enclosure is used for the temperature rise tests. Figure 3.1 shows a sketch of the RMU enclosure with dimensions and definitions of the surfaces. In this report, the side where the switchgear normally is operated from is defined as the back wall.

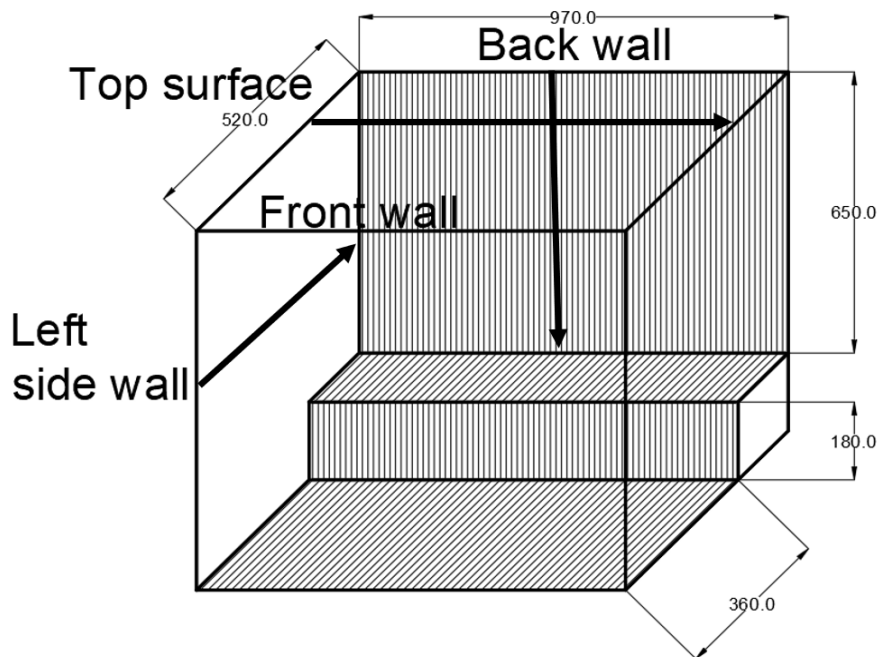


Figure 3.1 – Overview of the RMU enclosure with dimensions and explanations

Figure 3.2 shows a picture of the enclosure seen from the front. The content in the red circle in Figure 3.2 are components used to make the current path stable. These components are not expected to not affect the results of the experiments. Their only purpose is to make sure the current path is stable.

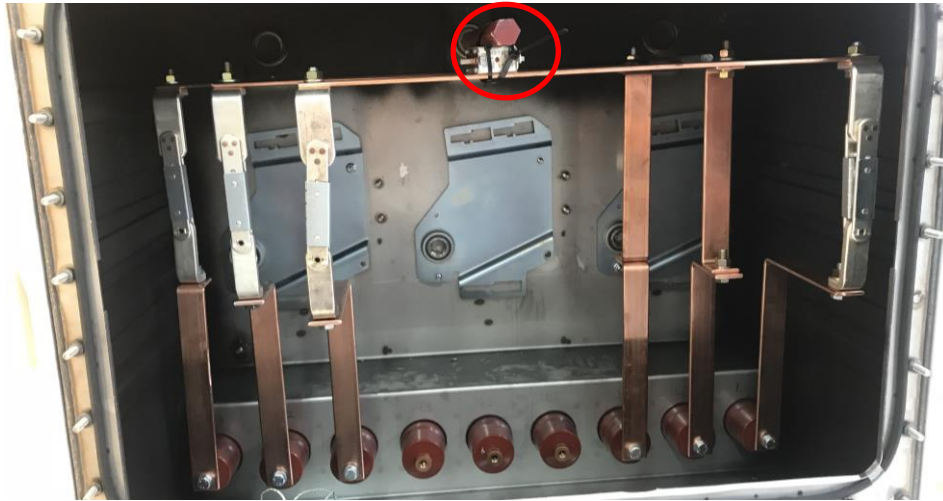


Figure 3.2 – Picture of the enclosure seen from the front wall

The test device in Figure 3.2 differs from a real design of switchgear. There are less components involved in the current path and less equipment used for supportive purposes. The mechanisms to operate the switchgear are neither involved in the test device. These differences between the test device and a real switchgear are most likely to affect the heat transfer within the enclosure.

Figure 3.3 shows a drawing of the isolated current path, the path is divided into a left and right module. The right module is connected to the power source and the left module are short-circuited with a copper bar at the outside-bushings.

The left module consists of one switch in each phase, while the right module consists of one switch in phase L1 and replacement bars in phase L2 and L3.

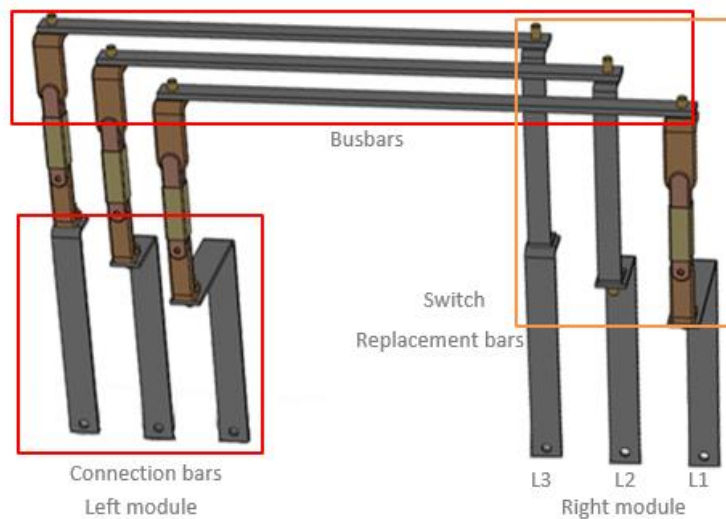


Figure 3.3 – Detailed drawing of the current path in the RMU enclosure

System description

3.1.2 Small enclosure

Figure 3.4 shows the small enclosure that fits exactly one switch. This enclosure is only used for mounting the switches while performing resistance measurements.



Figure 3.4 – Overview of the small enclosure that fits exactly one switch

3.2 Switches

The test device consists of four identical switches and two replacement bars. The replacement bars are intended to simulate the characteristics of the switch. Ideally, the test device should consist of six switches. The reason there is four switches are because the manufacturer produced four functional switches to perform a different experiment. When this experiment was completed, the switches was given to USN. The four switches are named based on their location in the RMU enclosure, such as “Switch L1 Right”.

The switches are made of silver-coated copper and the replacement bars are made of bare copper. Figure 3.5 shows a drawing of the replacement bar. Figure 3.6 shows a drawing of the switch with named individual parts.

Dimensions of the switch and replacement bar are given in Appendix D.



Figure 3.5 – Drawing of the replacement bar

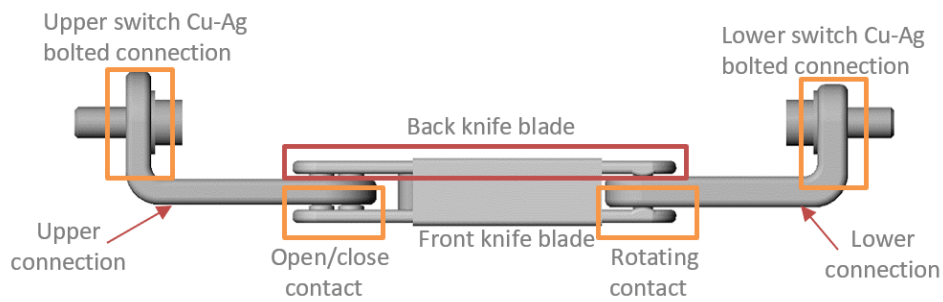


Figure 3.6 - Detailed drawing of the knife switch

Figure 3.6 shows that the switch is basically a parallel circuit with contact resistances and bulk resistances. The corresponding circuit diagram is shown in Figure 3.7, the explanations of the resistances occurring in the circuit is given below the circuit diagram.

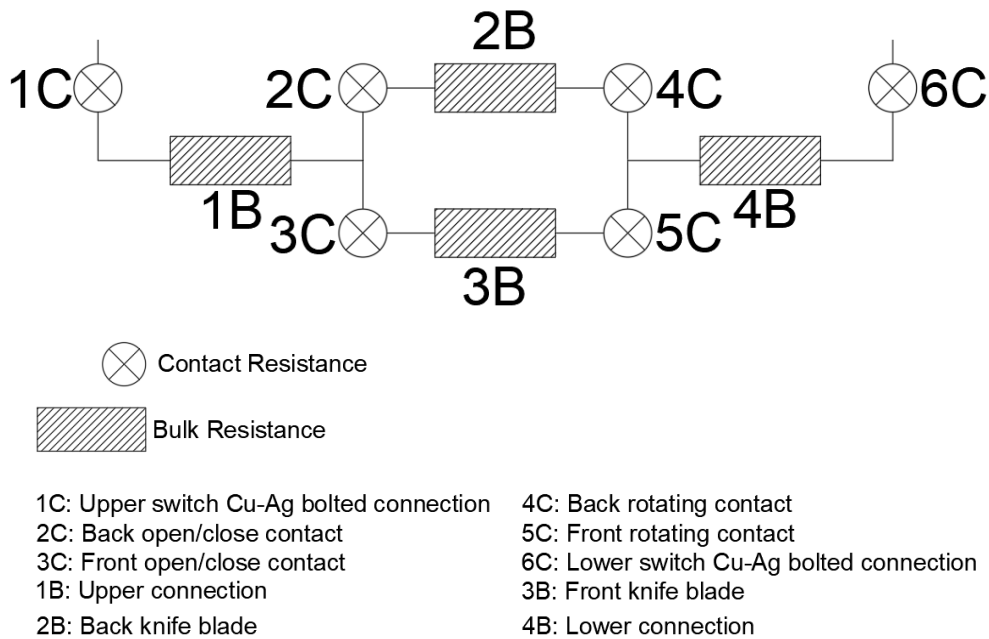


Figure 3.7 – Single line drawing of the switch with explanations

The ideal situation is for the current to divide equally between the contact resistances 2C and 3C, but due to the differences in the a-spots as described in chapter 2.1.1, there will always be minor differences in the contact resistances. Which could result in an unsymmetrical deviation of the current. Throughout this report, the current is assumed to divide equally between the front and back knife.

3.3 Conductors

Figure 3.8 shows the conductors going from the bushings to the switch connections. These bars have different lengths in order to make the current path as easy as possible. There are three pairs, one pair for each phase. The connection bars are mounted to the bushings in one end and to the switch in the other end using bolts, nuts and washers. All the bolted connections in the enclosure is tightened with a torque of 35Nm,



(a) Connection bar for phase L1 (b) Connection bar for phase L2 (c) Connection bar for phase L3

Figure 3.8 – Drawing of the connection bars from the bushings to the switches

Figure 3.9 shows the busbar connecting the left module to the right module at the top of the enclosure. The busbar has the same dimensions for each phase. The busbar is mounted to the switches or replacement bars in both ends with bolts and washers. The bolted connections in both ends are tightened with a torque of 35Nm.



Figure 3.9 – Drawing of the busbar

Dimensions of the conductors and busbar are given in Appendix D.

4 Performance of the experiments

In this chapter, the equipment needed to perform the measurements are presented, the procedure for assembling the test device and the performance of the experiments are described.

4.1 Equipment for measuring

Table 4.1 shows the equipment that is used for performing the experiment and the measurements conducted in this report. The equipment is provided by USN.

Table 4.1 – Equipment used in the experiment for measuring and control

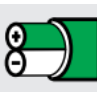
Equipment:	Fabricator:	Type:	Accuracy:
Current Injector	Hilkar	Ak23	
Voltmeter	Gossen Metrawatt	High Resolution TRMS System Multimeter	Voltage DC – for $60\text{ mV} \pm 30\text{ }\mu\text{V}$
Thermocouples [8]		Type K	$\pm 0,004\text{t}$ or $\pm 1,5^\circ\text{C}$
Logging device	Keysight	Agilent 34972A LXI Data Acquisition/ Switch unit Software: BenchLink Data Logger 3	
Manual thermometer	Fluke	54 II B	
<i>Clip-on current transformer*</i>	<i>Gossen Metrawatt</i>	<i>Z3512</i>	$\pm(0,5\text{ reading} + 0,05\text{A})$

**Intendent to use, not used*

4.1.1 Thermocouples and logging device

For measuring the temperatures, thermocouples have been used. Table 4.2 shows the specifications of the thermocouples. The thermocouples consist of two different semiconductors. The two semiconductors are in contact with each other at the location where the temperature is desirable, and a small electric charge is created. The temperature of this point determines the electric charge, which can be read using a manual thermometer or a logging device. Both a manual thermometer and a logging device is used in the experiments.

Table 4.2 – Thermocouple type K specifications [8]

	Element type	Class	Standard range
	K (Ni-Cr)	1	-40/1000°C

The locations of the thermocouples are decided in accordance with ABB and the supervisors, and it is thought of where the temperatures are reaching the highest values and what is needed to get a satisfying result.

Figure 4.1 shows an illustration of some of the positions to the thermocouples located on the current path of phase L1. The numbers represent the sensor label of a given thermocouple, Table 4.3 contains the sensor label and description of all the thermocouples located at the current path for all three phases.

The temperatures of the contacts in the switches are very relevant and phase L1 is the only phase containing a switch in each module, and therefore contains thermocouples at the same positions in both modules. Phase L2 and L3 do not have thermocouples at the replacement bars in the right module. The temperature of the air inside the top, the middle and the bottom of the enclosure is logged.

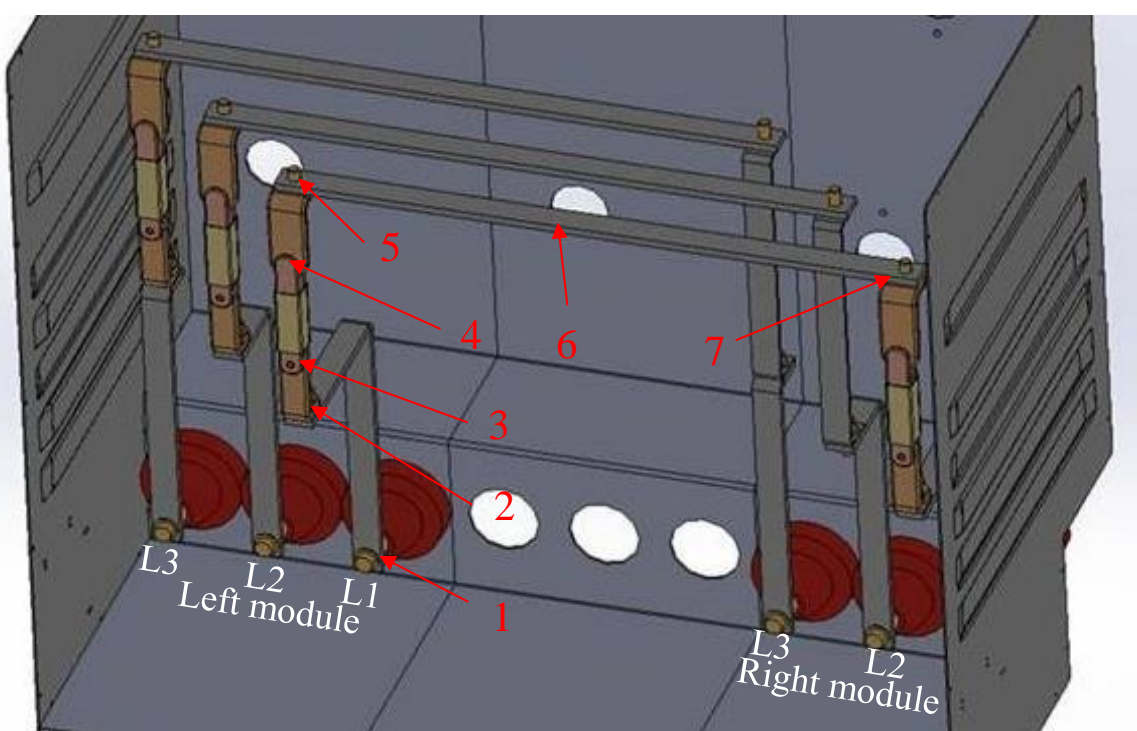


Figure 4.1 – Illustration of some of the locations of the thermocouples as described in Table 4.3

In addition to the thermocouples given in Table 4.3, temperatures of selected surfaces requested by the working group A3.36 are logged. The sensor label and description these are given in Appendix B.

Performance of the experiments

Table 4.3 – Positions of the thermocouples along the current path

Sensor	Position and description	Module
Phase L1		
1	Bushing connection Cu-Cu bolted connection	Left
2	Lower switch connection Cu-Ag bolted connection	Left
3	Rotating contact	Left
4	Open/Close contact	Left
5	Upper switch connection Cu-Ag bolted connection	Left
6	Middle of busbar	
-	<i>Near upper switch Cu-Ag bolted connection*</i>	<i>Right</i>
7	Upper switch connection Cu-Ag bolted connection	Right
8	Open/Close contact	Right
9	Rotating contact	Right
10	Lower switch connection Cu-Ag bolted connection	Right
11	Bushing connection Cu-Cu bolted connection	Right
Phase L2		
12	Bushing connection Cu-Cu bolted connection	Left
13	Lower switch connection Cu-Ag bolted connection	Left
14	Rotating contact	Left
15	Open/Close contact	Left
16	Upper switch connection Cu-Ag bolted connection	Left
17	Middle of busbar	
-	<i>Near upper switch Cu-Ag bolted connection*</i>	<i>Right</i>
29	Bushing connection Cu-Cu bolted connection	Right
Phase L3		
31	Bushing connection Cu-Cu bolted connection	Left
18	Rotating contact	Left
19	Open/Close contact	Left
32	Middle of busbar	
30	Bushing connection Cu-Cu bolted connection	Right

**These thermocouples were mounted after the first steady state temperature rise*

4.1.2 Mounting of the thermocouples

The thermocouples are mounted differently depending on their location. Figure 4.2 shows how the thermocouples are placed under the washers beneath the bolt. This mounting mechanism is used for all the bolted connections to read the temperature as close to the connection as possible. This kind of mounting could make the temperatures that are logged higher than results from similar experiments, where the thermocouples are mounted some millimeter from the bolt with tape and strips.

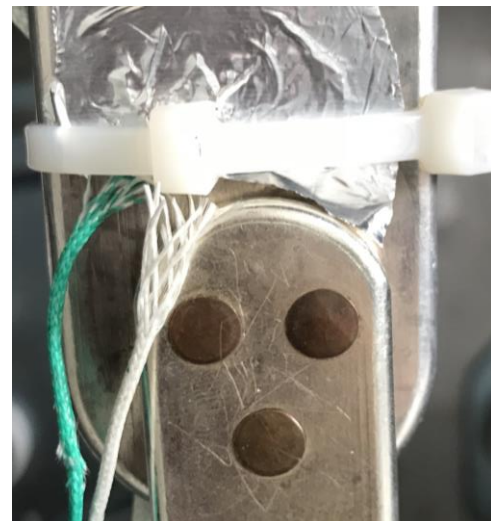


Figure 4.2 – Mounting of thermocouple using the washers beneath the bolt

The thermocouples used to log the temperatures of the rotating contacts and open/close contacts are held in place by strips and tape. Figure 4.3 a) shows how the thermocouple is mounted on the rotating contact and Figure 4.3 b) shows the thermocouple of the open/close contact.



(a) Thermocouple on the rotating contact



(b) Thermocouple on the open/close contact

Figure 4.3 – Mounting of thermocouple using strips and tape

Performance of the experiments

The thermocouples used to measure the temperature of the air inside the enclosure are located in the center between the sidewalls. There are three thermocouples used for measuring the air temperature, near the top, in the middle and near the bottom of the enclosure. The top surface is used as a reference for the heights of the thermocouples. Figure 4.4 shows the height of the top sensor, the middle sensor and the bottom sensor from the top surface.

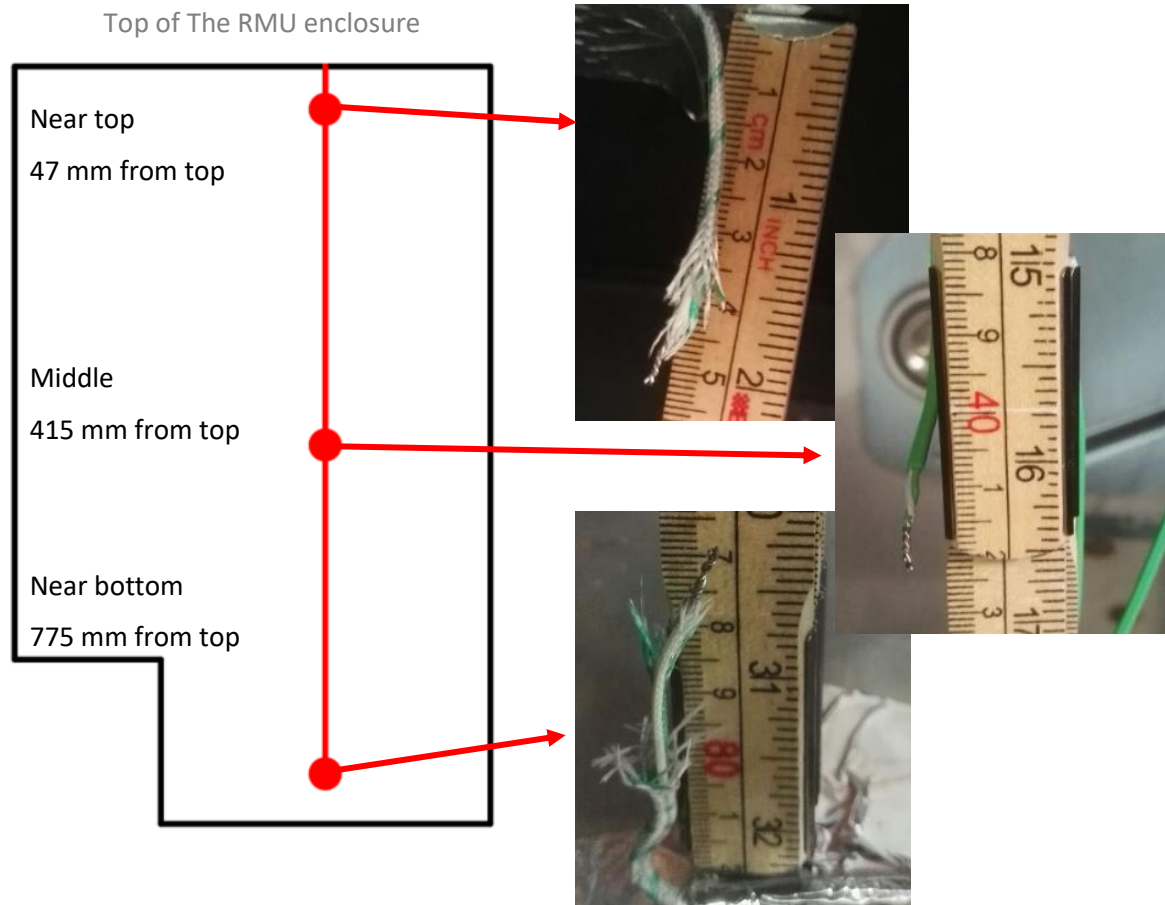


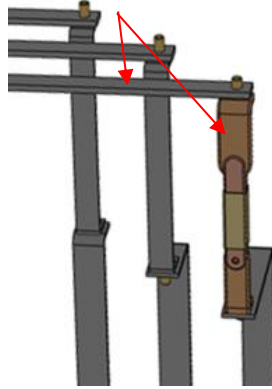
Figure 4.4 – Location of the thermocouples used for measuring the air temperature in the RMU enclosure, seen from the side

In Appendix B a detailed list and description of all the thermocouples are given.

4.1.3 Additional thermocouples for test 2 with nonmagnetic bolts

In test 2, two extra thermocouples were added to the current path to investigate if the mounting mechanism had impact on the temperatures that were read. Figure 4.5 shows a drawing of where these thermocouples are located. The thermocouples are mounted using tape and strips a few millimeters from the upper switch Cu-Ag bolted connection in the right module, the mounting is similar of the rotating contacts and open/close contacts.

Near upper switch Cu-Ag bolted connection



Right module

Figure 4.5 – Location of the additional thermocouples for test 2

4.2 Procedure for installing the setup

Figure 4.6 shows a picture of the finalized test device. The test device was assembled at the High Current Laboratory at USN in Porsgrunn.

The RMU enclosure that is used to conduct the experiment had components inside from previous test and parts of the inside surfaces were painted matt black. In order to assemble the test device, the student first removed the original components. Then the inside top surface and side walls were repainted matt black. To finalize the setup the student installed the components described in chapter 3. The openings shown in the middle of the picture in Figure 4.6 are closed after the picture were taken. The enclosure has no ventilation during experiments.

In Figure 4.6 the thermocouples used for measuring the temperatures are mounted along the current path. Description of the thermocouples and how they're mounted was given in chapter 4.1.1. Figure 4.7 shows one of the switches placed in the small enclosure.



Figure 4.6 – Picture of the finalized test device seen from the front



Figure 4.7 – Picture of one of the switches mounted between the bushings inside the small enclosure

4.3 Resistance and power loss measurements

For all resistance measurements, a stable DC current of 100A is used to measure the voltage drop over the part of interest. The magnitude of the current is not large enough to heat the switchgear to impact the resistance measurements. The voltage drop is denoted and converted to Ohms using Ohm's law.

4.3.1 Bulk resistance of the switch

The bulk resistance of the switches is measured during reference temperature (room temperature), the switches are mounted in the small enclosure. All the four switches are placed in the small enclosure in succession and the voltage is measured over the individual parts with the voltmeter.

4.3.2 Contact resistances of the switch

The contact resistances of the switch are measured during reference temperature when the switches are mounted in the small enclosure. All the four switches are placed in the small enclosure in succession and the voltage drop over each contact are measured with the voltmeter.

The contact resistances are measured again during reference temperature after the test device is finalized (when the switches and bars are assembled in the RMU enclosure). The voltage drop over each contact is measured with the voltmeter. These measurements are mainly executed to verify the results from the previous contact resistance measurement from the small enclosure, the contacts are then adjusted if there are large deviations between the measurement results from the small enclosure.

4.3.3 Total resistance of the current path inside RMU enclosure

The total resistance of the current path of the RMU enclosure during reference temperature is measured. The voltage drop over each individual part is measured, including the contact resistances where applicable. The resistance over the total phases are also measured, the voltage drop is measured from the outside bushing- to bushing connection.

4.3.4 Total resistance during steady state temperature

The total resistance of the current path is measured when the test device has reached steady state temperature (temperature rise less than 1°C per hour). The voltage drop over the outside bushing- to outside bushing connection is measured during steady state temperature. The current injector is set to deliver 630A AC at 50Hz to heat the test device up to steady state temperature.

To measure the resistance during steady state temperature, the AC power source is disconnected, and the DC power source is connected to avoid any influence from possible induced voltages caused by the changing magnetic field in AC. When the RMU enclosure is disconnected from the AC power source the temperature immediately starts to decrease, this will cause an error in the measured resistance. The DC power source is connected as fast as possible, and the resistances are measured within 2-3 minutes after the AC source is

disconnected. The measured resistance is therefore somewhat lower than the actual steady state resistance.

4.3.5 Power loss

The power loss of the switchgear is estimated during steady state temperature. Originally, the power loss from outside left bushing to right bushing were supposed to be measured with a clip-on current transformer and wattmeter.

The wattmeter intended for this purpose has limitations in the range of its measuring scale. The wattmeter demands a minimum voltage of 0,15V to measure power according to the user manual, which means for a current of 630A the resulting resistance must be at least $238\mu\Omega$ [12].

During steady state conditions the voltage for phase L1 is higher than the minimum limit of 0,15V, but the wattmeter does not respond. This implies that the minimum demands given in the user manual is not absolute and that the wattmeter is sensitive for the low voltages around this limit.

To estimate the power loss, equation (2.4) is used instead of the wattmeter. This method has shown good accuracy in previous experiments [9].

4.4 Temperature rise measurements

Two individual temperature rise tests are executed for the RMU enclosure. Test 1: magnetic bolts and test 2: nonmagnetic bolts.

4.4.1 Steady state temperatures test 1: magnetic bolts

In test 1, the bolts at the inside bushing connections in the RMU enclosure are made of magnetic material. The current injector is used to heat up the switchgear. This was set to deliver an AC current of 630A at 50Hz for all the three phases.

The temperatures of the described thermocouples are logged.

The results of the steady state air temperature inside the RMU enclosure are compared to the estimated air temperatures found by the IEC model described in Chapter 2.4. The temperatures along the current path are used to calculate the heat transfer coefficient.

4.4.2 Steady state temperatures test 2: nonmagnetic bolts

In test 2, the bolts and washers at the inside bushing connections in the RMU enclosure are made of nonmagnetic material. The current injector is used to heat up the switchgear. This was set to deliver an AC current of 630A at 50Hz for all the three phases, similar to test 1.

Figure 4.8 shows which of the bolts and washers that are replaced before test 2 is conducted.



Figure 4.8 – Picture of which bolts and washers that are replaced during test 2

The same temperatures logged in test 1 are logged for test 2. The temperatures of the air inside the RMU enclosure are logged until steady state temperature was reached. The temperatures along the current path are logged until steady state was reached. In addition, the extra thermocouples as describes in Chapter 4.1.3 are logged when steady state temperature is reached.

4.4.3 Temperatures requested by the working group

The temperatures of the inside and outside side wall, front wall and top surface is logged when steady state temperature is reached. The temperatures of the power cables 1 meter and 2 meters from the bushings are measured during steady state conditions. These temperatures were explicitly requested by the external partner of the thesis. The exact locations of the measuring point of the surfaces are given in Appendix B and the temperatures of these locations are given in Appendix C.

5 Resistance and power loss

In this chapter, the results from the resistance and power loss calculations and measurements are presented and discussed.

5.1 Bulk resistance results

The theoretical bulk resistance of the current path that is calculated and measured is presented in the next subchapters. When calculating the bulk resistance, the specific resistance could contribute to inaccuracy. The value of the specific resistance that is used could deviate from the actual parameter of the material, resulting in a deviation between the measured and calculated resistance. The specific resistance is as mentioned in Chapter 2, hard copper ($\rho = 0,01786$).

5.1.1 Theoretical bulk resistance of the knife switch and replacement bar

The calculations are assumed reference temperature (room temperature). The switch is divided by the individual parts shown and described in Chapter 3.2. Equation (2.2) is used to calculate the bulk resistance.

Table 5.1 shows the dimensions, cross section and resulting bulk resistance of the switch.

Table 5.2 shows the dimensions, cross section and bulk resistance of the replacement bar.

Table 5.1 – Calculation of the theoretical bulk resistance of the knife switch

Part No:	Length	Width	Depth	Cross section	Bulk resistance
	[mm]	[mm]	[mm]	[mm ²]	[$\mu\Omega$]
Upper connection	110	27	9	243,0	8,1
Back knife	120	25	4	100,0	21,4
Front knife	120	25	4	100,0	21,4
Lower connection	130	37	7	259,0	9,0
Total bulk resistance $R_{Bulk-switch}$	-	-	-	-	27,8

Table 5.2 – Calculation of the theoretical bulk resistance of the replacement bar

	Length	Width	Depth	Cross section	Bulk resistance
	[mm]	[mm]	[mm]	[mm ²]	[$\mu\Omega$]
Replacement bar	330	40	6	240,0	24,3

The theoretical bulk resistance of the switch and replacement bar in Table 5.1 and

Table 5.2 are based on the dimensions and material of the component. The dimensions of the switch are found using a caliper, which is a precision instrument and the small errors that could occur using this instrument are negligible. Dimensions of the replacement bar is given by the manufacturer.

In Appendix D the excel sheets used for calculation of the bulk resistances is given.

5.1.2 Theoretical bulk resistance of the conductors

The bulk resistance in the connection bars is different for each phase, due to different lengths of the connection bars. The busbars on the top of the enclosure are identical for the three phases.

Table 5.3 shows the length, cross section and the resulting bulk resistance for the connection bars. Table 5.4 shows the length, cross section and resulting bulk resistance of the busbar.

Table 5.3 – Theoretical bulk resistance of the connection bars

Phase:	Length	Cross section	Bulk resistance
	[mm]	[mm ²]	[μΩ]
L1	470	240,0	34,2
L2	370	240,0	27,0
L3	330	240,0	24,3

Table 5.4 – Theoretical bulk resistance of the busbars

	Length	Cross section	Bulk resistance
	[mm]	[mm ²]	[μΩ]
Busbar	650	240,0	47,5

The theoretical bulk resistances of the conductors are dependent on the same conditions as the theoretical bulk resistance of the switches and replacement bars. The dimensions of the conductors are given by the manufacturer, and the specific resistance of these are determined to be equal to the specific resistance of the switch.

In Appendix D, the excel sheet used for calculation of the bulk resistances is given.

5.1.3 Measured bulk resistance of the switch

Table 5.5 shows the measured bulk resistance of the switches during reference temperature when they are placed in the small enclosure. The bulk resistance of each individual part of the switch is measured and summed together.

Table 5.5 – Measured bulk resistance of each switch in the small enclosure during reference temperature

Switch No	Module	Bulk resistance [$\mu\Omega$]
Switch L1	Right	26,0
Switch L1	Left	26,3
Switch L2	Left	29,8
Switch L3	Left	25,8
Average		27,0

The average bulk resistance in Table 5.5 and the theoretical bulk resistance of the switch in Table 5.1 are very close. This implies that the specific resistance factor is chosen correctly.

5.2 Contact resistance results

The contact resistances that are measured is presented in the next subchapters.

5.2.1 Measured contact resistances of the switch placed in the small enclosure

Figure 5.1 shows the maximum and minimum contact resistances that appear when the switches are placed in the small enclosure. The x-axis is given as the switch. The y-axis is given as the resistance. This gives an idea of where the biggest variation in the resistance occur. Table 5.6 shows exact values as shown in the graphical illustration in Figure 5.1.

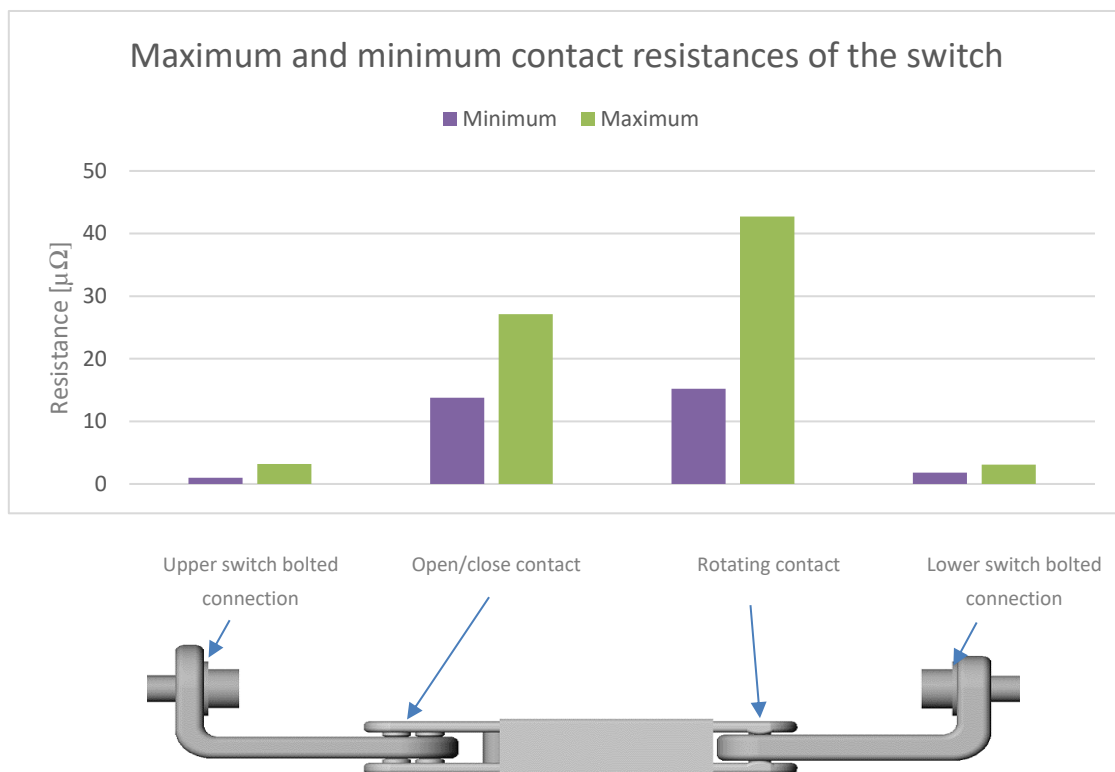


Figure 5.1 – Graphical representation of the measured contact resistance of the switches in the small enclosure

Table 5.6 – Measured minimum and maximum contact resistance of the switches placed in the small enclosure

Part No:	Minimum [$\mu\Omega$]	Maximum [$\mu\Omega$]	Average [$\mu\Omega$]
Upper contact	1,0	3,2	1,5
Open/close contact	13,8	27,1	16,5
Rotating contact	15,2	42,7	23,7
Lower contact	1,8	3,1	2,4
Sum	17,3	41,2	24,0

Resistance and power loss

The contact resistances of the switch in the small enclosure from Figure 5.1 shows large variations, especially in the open/close contact and the rotating contact. Table 5.6 shows that the contact resistance of the rotating has the highest value, and varies with $\pm 27,5\mu\Omega$.

In Appendix E the excel sheet for the contact resistance measurements in the small enclosure is given.

5.2.2 Contact resistances of the current path placed in the RMU enclosure

Table 5.7 shows the measured contact resistances of the switches and the bolted contacts of the current path in the RMU enclosure.

Table 5.7 – Measured contact resistances of the switches and the bolted contacts inside the RMU enclosure

	Module	L1 [$\mu\Omega$]	L2 [$\mu\Omega$]	L3 [$\mu\Omega$]
Bushing Cu-Cu connection bolted	Left	3,6	2,2	3,1
Lower switch Cu-Ag connection	Left	4,7	3,9	1,9
Rotating contact				
<i>front</i>	Left	12,0	12,4	10,2
<i>back</i>	Left	13,6	12,7	8,5
Open/Close contact				
<i>front</i>	Left	9,3	7,2	8,0
<i>back</i>	Left	8,2	8,0	11,5
Upper switch Cu-Ag connection	Left	2,6	1,9	2,3
Bushing Cu-Cu connection bolted	Right	2,4	1,1	1,5
Lower switch Cu-Ag connection	Right	3,2	2,5	1,0
Open/Close contact				
<i>front</i>	Right	7,2	-	-
<i>back</i>	Right	8,1	-	-
Rotating contact				
<i>front</i>	Right	32,0	-	-
<i>back</i>	Right	23,0	-	-
Upper switch Cu-Ag connection	Right	1,9	1,2	3,3
Sum		46,3	22,86	22,45

Table 5.7 shows that when the switches are placed inside the RMU enclosure the contact resistances of the switches decreases from the results in Table 5.6. But the resistance of the rotating contact is still larger than the contact resistance of the open/close contact.

The large contact resistance of the rotating contact is unexpected. In the report “Power loss and temperature rise measurements in a four-module switchgear” the average resistance of a rotating contact is found to be $1,6\mu\Omega$. The average resistance of an open/close contact is found to be $3,2\mu\Omega$ [13]. The contact resistances of the rotating contact and the open/close contact in the RMU enclosure are considerably higher than the average values found in the report.

The contact resistances of the bolted connections vary between $1-5\mu\Omega$ when 35Nm is used for tightening the nuts. In the report “Power loss and temperature rise in a four-module switchgear”, the average contact resistance of bolted contacts are measured to be between $1,1\mu\Omega$ and $2,5\mu\Omega$ [10]. This is in the same order as the resistances for the bolted contacts in the test device.

5.3 Total resistance results

The total resistance of the current path inside the RMU enclosure are measured. The sum of the theoretical bulk resistance is first presented, then the sum of individual measurements from the current path is presented and the measurement from the bushing to bushing.

5.3.1 Total theoretical bulk resistance of the current path

Table 5.8 shows the total theoretical bulk resistance of the current path of the RMU enclosure.

Table 5.8 – Total theoretical bulk resistance of the current path of the RMU enclosure

Part No:	Module:	L1 [$\mu\Omega$]	L2 [$\mu\Omega$]	L3 [$\mu\Omega$]
Connection bar	Left	34,2	27,0	24,3
Switch	Left	27,8	27,8	27,8
Busbar		47,5	47,5	47,5
Switch/Replacement bar	Right	27,8	24,3	24,3
Right module	Right	34,2	27,0	24,3
Sum bulk resistance		171,5	153,6	148,2

Table 5.8 shows that the total theoretical bulk resistance of the enclosure is $473\mu\Omega$.

5.3.2 Measured total resistance of the current path inside RMU enclosure

Table 5.9 shows the measured resistance if the individual parts of the current path inside the RMU enclosure.

Table 5.9 – Measured resistance of the individual conductors of the current path of the RMU enclosure

	Module	L1 [$\mu\Omega$]	L2 [$\mu\Omega$]	L3 [$\mu\Omega$]
Connection bar*	Left	37,7	28,7	22,9
Switch	Left	48,2	47,5	48,0
Busbar*		48,8	47,9	48,6
Switch/replacement bar	Right	48,2	26,2	25,9
Connection bar*	Right	36,3	26,1	23,1
Sum resistance		219	176	168

**These values include the contacts resistances of the bolted connections of the endings*

In the report “Heat transfer mechanisms in MV load break switches” the cold resistance of a knife switch was found to be $35\mu\Omega$ [14].

Table 5.10 shows the total resistance of the current path of the RMU enclosure before and after the enclosure are heated up to steady state air temperature.

Table 5.10 – Measured total resistance of each phase for the RMU enclosure

	Resistance at reference temperature, before heating [$\mu\Omega$]	Resistance at reference temperature, after heating [$\mu\Omega$]
L1	218	195
L2	173	162
L3	163	158
Total	554	515

The resistance is reduced with 7% after heating, this is in accordance with previous results.

The theoretical bulk resistance of the individual conductors in Table 5.8 agrees with the measured total resistances in Table 5.9. The theoretical bulk resistances in Table 5.8 is lower than the measured resistances, this is because the theoretical values do not include the contact resistance.

The sum of the individual measurements in Table 5.9 are a little larger than the total resistance measurements from the outside bushing-to-bushing in Table 5.10, this is probably because parts of some of the resistances are included in several measurements.

The report “Power loss measurement and temperature rise in a four-module switchgear” measured the resistance of one phase to be about $180\mu\Omega$ [13]. In the paper “Thermal design of future medium voltage switchgear”, the total resistance is measured to be $639\mu\Omega$ [6]. The total resistance of the test device is between the results from these two reports.

5.4 Resistance during steady state temperature results

5.4.1 Estimated increase in resistance with temperature rise

Figure 5.2 shows how the measured resistance before heating from Table 5.10 at reference temperature increases when the temperature rises. The x-axis is the temperature rise. The y-axis is given as the resistance. The point of congelation is moved to $100\mu\Omega$ on the y-axis for better visualization.

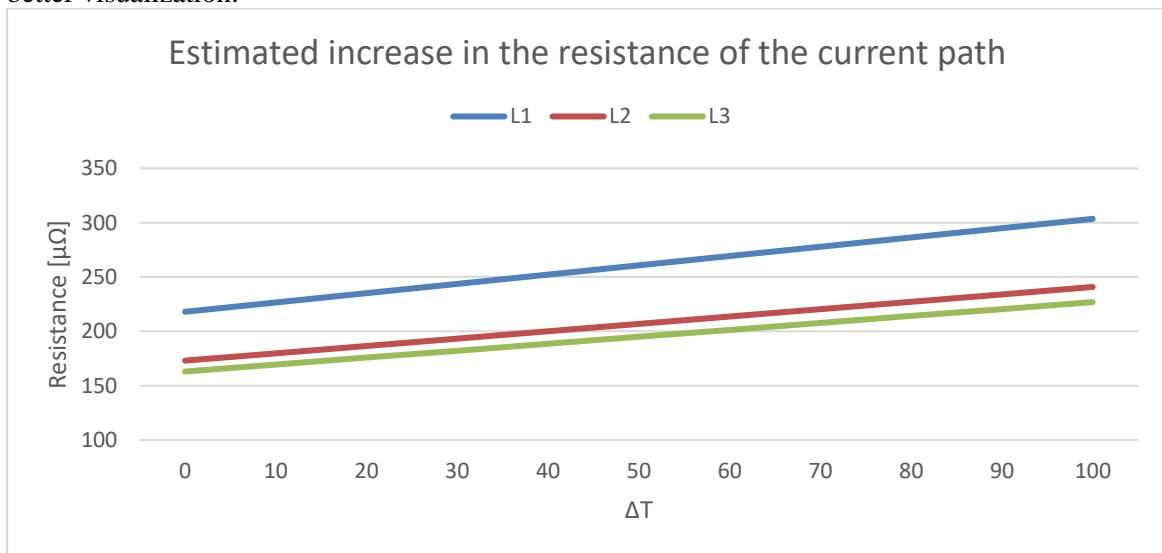


Figure 5.2 – Estimation of increase in temperature based on the measured total resistance from Table 5.10

In Appendix F, the excel sheet for the estimation of the increase in resistance is given.

5.4.2 Measured resistance at steady state temperature

Table 5.11 shows the steady state temperature resistance of the RMU enclosure for test 1 and test 2.

Table 5.11 – Measured total resistance of the RMU enclosure during steady state temperature

	Test 1: Magnetic bolts		Test 2: Nonmagnetic bolts	
	Resistance [$\mu\Omega$]	Temperature rise* [°C]	Resistance [$\mu\Omega$]	Temperature rise* [°C]
L1	283,2	91,7	277,6	86,5
L2	241,4	89,9	242,3	84,3
L3	221,1	88,5	213,4	84,0
Total	745,7	-	733,3	-

*Temperature rise of the middle busbar for the respective phases

5.5 Power loss estimate

Table 5.12 shows the estimated power loss from the resistances found in Table 5.11. Equation (2.4) is used to estimate the power loss.

Table 5.12 – Estimation of the power loss of the current path in the RMU enclosure

	Test 1: Magnetic bolts	Test 2: Nonmagnetic bolts
	Power loss [W]	Power loss [W]
L1	112,4	110,2
L2	95,8	96,2
L3	87,7	84,7
Total	295,9	291,1

The power loss is just below 300W for the total current path for both tests. This is a little lower than previous test on similar switchgear. In the report “Heat transfer mechanisms in MV load break switches” the power loss was measured to be 340–350W [10].

5.6 Discussions

5.6.1 Bulk resistance

The theoretical and measured bulk resistance are in the same order. The deviation between the average measured and theoretical bulk resistance of the switch are less than 3%. This implies that the accuracy of the theoretical calculation of the bulk resistance are good, but strictly dependent on selecting the correct variable for specific resistance.

This small difference is probably related to dealing with the probes of the voltmeter. The probes are placed over the part of interest when taking the measurement, and the position of the probes will not be at the exact same location for each switch.

The bulk resistances for phase L1, L2 and L3 is calculated to be $171\mu\Omega$, $154\mu\Omega$ and $148\mu\Omega$ respectively.

5.6.2 Contact resistance

There were found large variations in the contact resistances of the rotating contacts and open/close contacts when the switches are placed in the small enclosure. The contact resistances of the rotating and open/close contacts decreases in some extent when the switches are placed in the RMU enclosure, but are still considerably larger than the average value found in the report “Power loss and temperature rise measurements in a four-module switchgear” [13]. It is important to emphasize that the switches used in the report “Power loss and temperature rise measurements” are not identical to the switches used in this experiment, and some difference is therefore obvious due to the a-spots. The large difference does however imply that the contact pressure of the rotating contacts and the open/close contacts are too low.

It was found that the resistance of the rotating contacts is larger than the resistance of the open/close contact in both the enclosures, this is an unexpected result. Previous result showed that the open/close contact had a larger contact resistance than the rotating contact [13]. The rotating contact is rotating around its own axis, and the two individual parts (back and front knife blade) is visibly always in contact with the lower connection (Figure 3.6). The open/close contact is the part of the switch that is breaking/making the current path and could be totally separated from the upper connection (Figure 3.6).

This finding implies that the contact pressure is lower for the rotating contact than for the open/close contact for the test device. In addition, the large variation between maximum and minimum value of the resistance of the rotating contact implies that the switches are vulnerable to changes (different positions). Each of the switches are mounted in the small enclosure and is visibly in the same position, but the a-spots may be different for each switch which seem to impact the resistance in a large extent.

When the switches are placed inside the RMU enclosure the resistance of the rotating contact decreases as shown in Table 5.7, but are still larger than the open/close contact resistance. The resistance of the open/close contact is decreased as well but is still in the same order as the results in Table 5.6 from the small enclosure. The decrease in the resistances could be due to better mounting of the switches and more stable positions in the RMU enclosure than in the small enclosure, lowering the possibility of changing the position of the knife blades. The

variation of the contact resistances could probably be reduced with some kind of supportive components and equipment, to make the contact pressure greater and position of contact more stable.

All the bolted contacts are fastened with the same torque in the RMU enclosure. The resistance of the bolted connections does therefore not vary as much as the rotating contacts and open/close contacts. The lower and upper switch Cu-Ag bolted connection have some variation between the maximum and minimum value but are in the same order as the resistances found in the report “Power loss and temperature rise measurements in a four-module switchgear” [13]. Small variations will occur due to the a-spots, as mentioned earlier. The resistance of the bolted connection is easier to manipulate, and by increasing the torque the resistance could be reduced.

The sum of the contact resistances for phase L1, L2 and L3 is measured to be $46\mu\Omega$, $23\mu\Omega$ and $22\mu\Omega$ for the current paths inside the RMU enclosure. The total contact resistance is about 16% of the total resistance of the test device, in the report “Power loss and temperature rise in a four-module switchgear” the total contact resistance was about 36% of the total resistance [13].

In the paper “Thermal design of future medium voltage switchgear”, the sum of the contact resistances is about 35% of the total resistance [6].

Figure 5.3 shows a graphical illustration of the relation between the bulk and contact resistance.

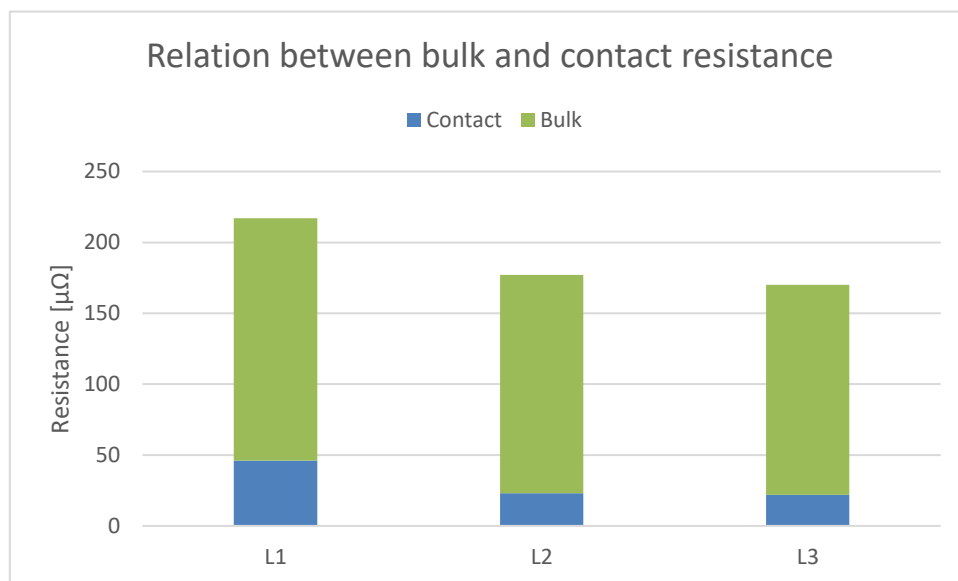


Figure 5.3 – Graphical illustration of the relation between the bulk and contact resistance

The contact resistance of phase L1 is about 21%, phase L2 is about 13% and phase L3 is about 13% of the total resistance.

There is less contact resistance in phase L2 and L3 than L1 because these phases only contain one switch. The amount of contact resistance are a little lower than the previous results.

5.6.3 Total resistance and power loss

The total resistance was measured to be $554\mu\Omega$ during reference temperature. Phase L1 has the highest resistance of $218\mu\Omega$, while phase L2 and L3 are $173\mu\Omega$ and $163\mu\Omega$, respectively.

The total resistance of the test device just above the total resistance from the report “Power loss measurement and temperature rise in a four-module switchgear”, and lower than the total resistance found in the paper “Thermal design of future medium voltage switchgear” [13] [9]. The different lengths of the connection bars in the phases makes the resistance of each phase different, the replacement bars in phase L2 and L3 reduces the resistance in these phases.

The total power loss of the test device is just below 300W for both tests. This is a little lower than previous test on similar switchgear. In the report “Heat transfer mechanisms in MV load break switches” the total power loss was between 340–350W [10]. Ideally the power loss of the test device should be a little higher to be realistic.

Based on the total measured resistance of the switch and the sum of the bulk resistance of the switches, the sum of the contact resistances of the switch could be estimated using the Equation (2.1). The total resistance of the switch from Table 5.9 and the average bulk resistance from Table 5.5 are used. The estimated sum of contact resistances in shown in Equation (5.1).

$$R_{Contact-Switch} = R_{Switch} - R_{Bulk-Switch} = 48,2\mu\Omega - 27\mu\Omega = 21,2\mu\Omega \quad (5.1)$$

The sum of the contact resistances of the switch is estimated to be 21μΩ. This is close to the average sum of the contact resistances of the switch from Table 5.6.

Equation (5.2) shows an estimate of the total contact resistance of phase L1. The estimation is assuming the contact resistance of the switch to be 21μΩ and using the contact resistance of the bushing connections from Table 5.7, the sum of the contact resistances of phase L1 gives a contact resistance of 48μΩ.

$$\begin{aligned} R_{Contact-Sum} &= (Bushing\ connection\ Cu - Cu\ Left) + 2 * R_{Contact-Switch} \\ &+ (Bushing\ connection\ Cu - Cu\ Right) \\ &= 3,6\mu\Omega + 2 * 21,2 + 1,9\mu\Omega = 48\mu\Omega \end{aligned} \quad (5.2)$$

With these assumptions, the sum of the contact resistances is about 22% of the total resistance of phase L1. This corresponds to the findings in Chapter 5.6.2, where the contact resistance is The total bulk resistance of phase L1 is 78% of the total resistance of phase L1.

This implies that the test device consists of a bit more bulk resistance than previous results from similar experiments, but the amount of contact resistance is still within the same order. The contact resistances of the rotating contact and the open/close contact did however have large variations. The contact resistance of the rotating contact was varying between 15,2μΩ and 42,7μΩ in the small enclosure, leaving the estimated sum of all the contact resistances from Equation (5.1) a bit larger than the average value.

The variation on the contact resistance of the rotating contact could impact the amount of contact resistance in the current path, in a worst-case scenario (when the contact resistance is at its maximum value of 42,7μΩ) the contact resistance of the rotating contact is 19,6% of the total resistance of the current path in phase L1.

Replacing the magnetic bolts and washers did not impact the power loss significantly, and therefore neither the resistance.

5.6.4 Resistance during steady state temperature

The total resistance of current path increased with 26% from reference temperature to steady state temperature. In the paper “Thermal design of future medium voltage switchgear”, the total resistance from reference temperature to steady state temperature increased with about 16% [6]. In the report “Power loss and temperature rise of a four-module switchgear” the increase in resistance is about 25% from reference temperature to steady state temperature [13].

The resistances measured during steady state conditions in Table 5.11 has a temperature rise between 84°C to 92°C. For test 1: magnetic bolts the total resistance is measured to be 746 $\mu\Omega$ and test 2: nonmagnetic bolts the total resistance is 733 $\mu\Omega$. Table 5.13 shows the estimated resistances from Figure 5.2 for temperature rises between 80°C and 100°C. Comparing the estimated steady state resistances and measured steady state resistance in

Table 5.13 and Table 5.11, there is a minor deviation between them. The deviation is probably due to the factors related to the material properties when estimating the resistance during steady state temperatures. The temperature coefficient is different for different materials, and using incorrect factor results in an error in the estimate.

Table 5.13 – Estimated increase in the resistance from Figure 5.2

ΔT [°C]	Resistance L1 [$\mu\Omega$]	Resistance L2 [$\mu\Omega$]	Resistance L3 [$\mu\Omega$]	Total Resistance [$\mu\Omega$]
80,0	286,3	227,3	214,1	727,7
90,0	294,9	234,0	220,5	749,5
100,0	303,5	240,8	226,9	771,2

However, the estimated “warm” resistances are in the same order as the measured “warm” resistance. There is probably some measuring error related to the steady state resistance measurement. To measure the steady state resistance the AC power supply must be disconnected, and the DC power supply connected. When the AC power supply is disconnected from the switchgear the temperature instantly starts do decrease. The measured resistance is therefore somewhat lower than the actual steady state temperature resistance.

6 Temperature rise

In this chapter, the results from the steady state temperature rise tests is presented and discussed. All temperatures given in this chapter are ΔT , temperature rise.

6.1 Estimate of air temperature inside RMU enclosure

This section contains the calculation of the expected air temperature rise. The IEC model as described in chapter 2.4 is used. The dimensions shown in Figure 3.1 is used to find the area A_0 of the enclosure. The surface factor b is found in Table 3 in the IEC report [7].

Table 6.1 shows the surface area, surface factor and the resulting cooling surface used to find the parameters in Table 6.2.

Table 6.1 – Area and surface factors for estimating the air temperature according to IEC method

	Area A_0 [m ²]	Surface factor b	Resulting cooling surface A_e [m ²]
Top	0,5044	1,4	0,7061
Back wall	0,6305	0,5	0,3152
2 * side wall	0,8056	0,5	0,4028
Bottom	0,3492	0	0
Front wall	0,8051	0,9	0,7245
Sum	3,0948		2,1488

The variables in Equation (2.6-2.7) from chapter 2.4 are shown in Table 6.2.

Table 6.2 – Variables for estimating the temperature rise

Variable	Value	Explanation
d	1,0	Factor for 0 numbers of horizontal partitions in Table 4 in IEC report [7]
k	0,275	Inserting A_e in graph in figure 3 in IEC report [7]
x	0,804	From table 1 in IEC report [7]
c	1,310	Inserting A_e in graph 1 in figure 4 in IEC report [7]

Table 6.3 shows the estimated air temperature at mid height and top height of the RMU enclosure. The temperatures are based on the power loss from test 1: magnetic bolts and test 2: nonmagnetic bolts from Table 5.12.

Table 6.3 – Estimated air temperature inside the RMU enclosure

	P_{loss} [W]	$\Delta t_{0,5}$ [°C]	$\Delta t_{1,0}$ [°C]
Test 1	295,9	27	35
Test 2	291,1	26	34

There is not a large difference between the estimated air temperature between test 1 and test 2, this is probably because there are only about 5W difference between the power loss of test 1 and test 2.

6.2 Air temperature inside the enclosure

The air temperature in top-height, mid-height and bottom-height are logged for both tests.

6.2.1 Measured steady state air temperature rise for test 1: magnetic bolts

Figure 6.1 shows a graphical representation of the air temperatures from test 1. The x-axis is given as the temperature rise, y-axis is given as a simplified drawing of the RMU enclosure seen from the front. The top-surface is used as the reference for the location of the thermocouples.

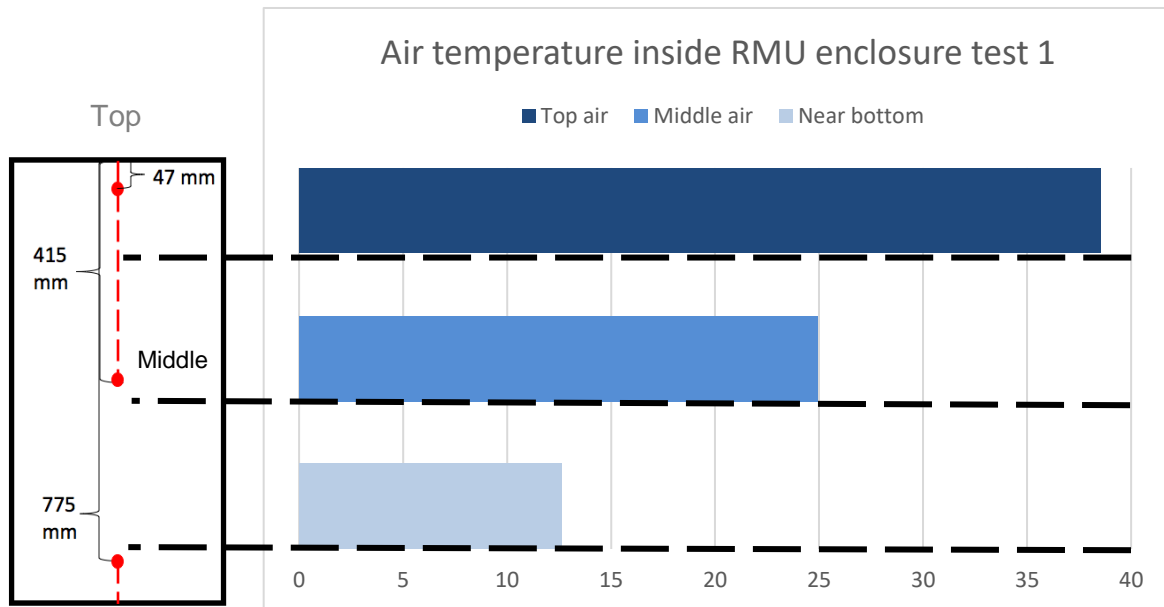


Figure 6.1 – Graphical representation of the steady state air temperature rise inside the RMU enclosure for test 1

The temperature near the bottom of the enclosure is significantly lower than the temperature near the top of the enclosure.

6.2.2 Measured steady state air temperature rise for test 2: nonmagnetic bolts

Figure 6.2 shows a graphical representation of the air temperature from test 2. The x-axis is given as the temperature rise, y-axis is given as a simplified drawing of the RMU enclosure seen from the front. The top-surface is used as the reference for the location of the thermocouples.

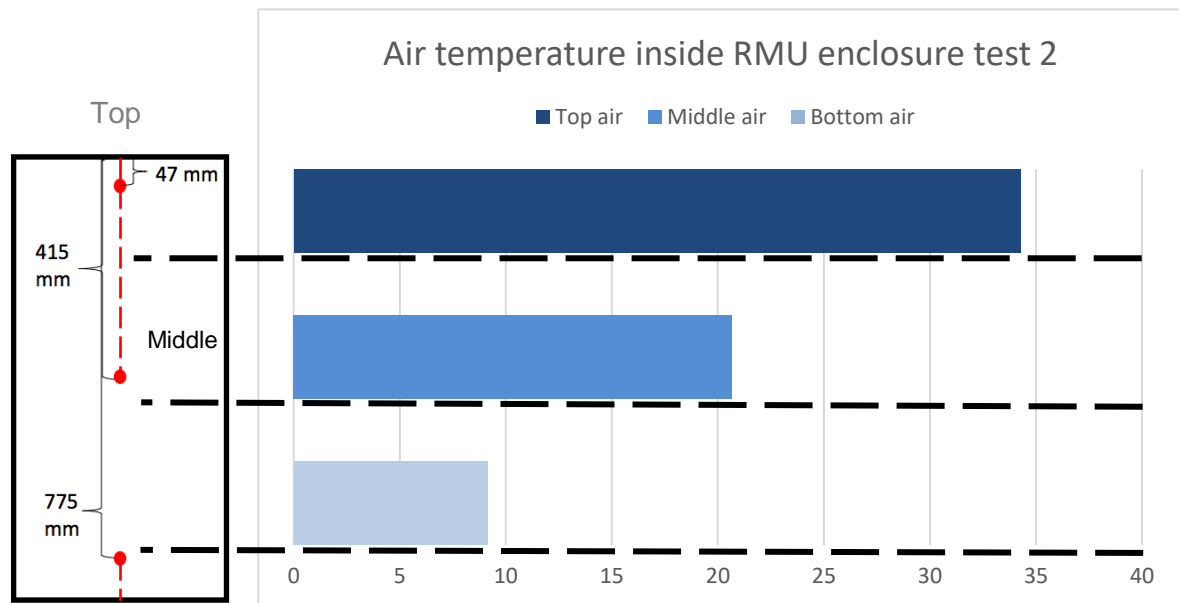


Figure 6.2 – Graphical representation of the steady state air temperature rise inside the RMU enclosure for test 2

6.2.3 Comparison of the steady state air temperature result of test 1 and test 2

Table 6.4 shows the results from the steady state air temperature of test 1 and test 2, along with the percentage reduction in the steady state temperature from test 1 to test 2.

Table 6.4 – Steady state air temperature inside RMU enclosure for test 1 and test 2

Sensor	Position and description	Test 1 ΔT [°C]	Test 2 ΔT [°C]	Percentage reduction from test 1
20	Inside air Near top of compartment	38,55	34,28	11,1 %
21	Inside air Middle of compartment	24,95	20,66	17,2 %
22	Inside air Near bottom of compartment	12,62	9,15	27,5 %

The complete list of the steady state air temperatures is given in appendix G.

In the report “Heat transfer mechanisms in MV load break switches” the temperature of the air inside the middle of the enclosure is measured to be about 30°C [11]. This temperature is a little higher than the temperatures measured in the mid-height of the test device.

6.3 Steady state temperature of the current path

This section contains the results from the steady state temperature measurements.

6.3.1 Measured steady state temperature of test 1: magnetic bolts

Figure 6.3 shows a plot of the steady state temperatures of the measuring points along the current path in test 1. The y-axis is given as the temperature rise. The x-axis is given as the switch, with names of the respective parts. The bushing connection at both endings are at the bottom of the enclosure, the busbar is the measuring point closest to the top surface.

The horizontal lines represents the maximum temperature rise limits for spring loaded and bolted contacts given by IEC [6].

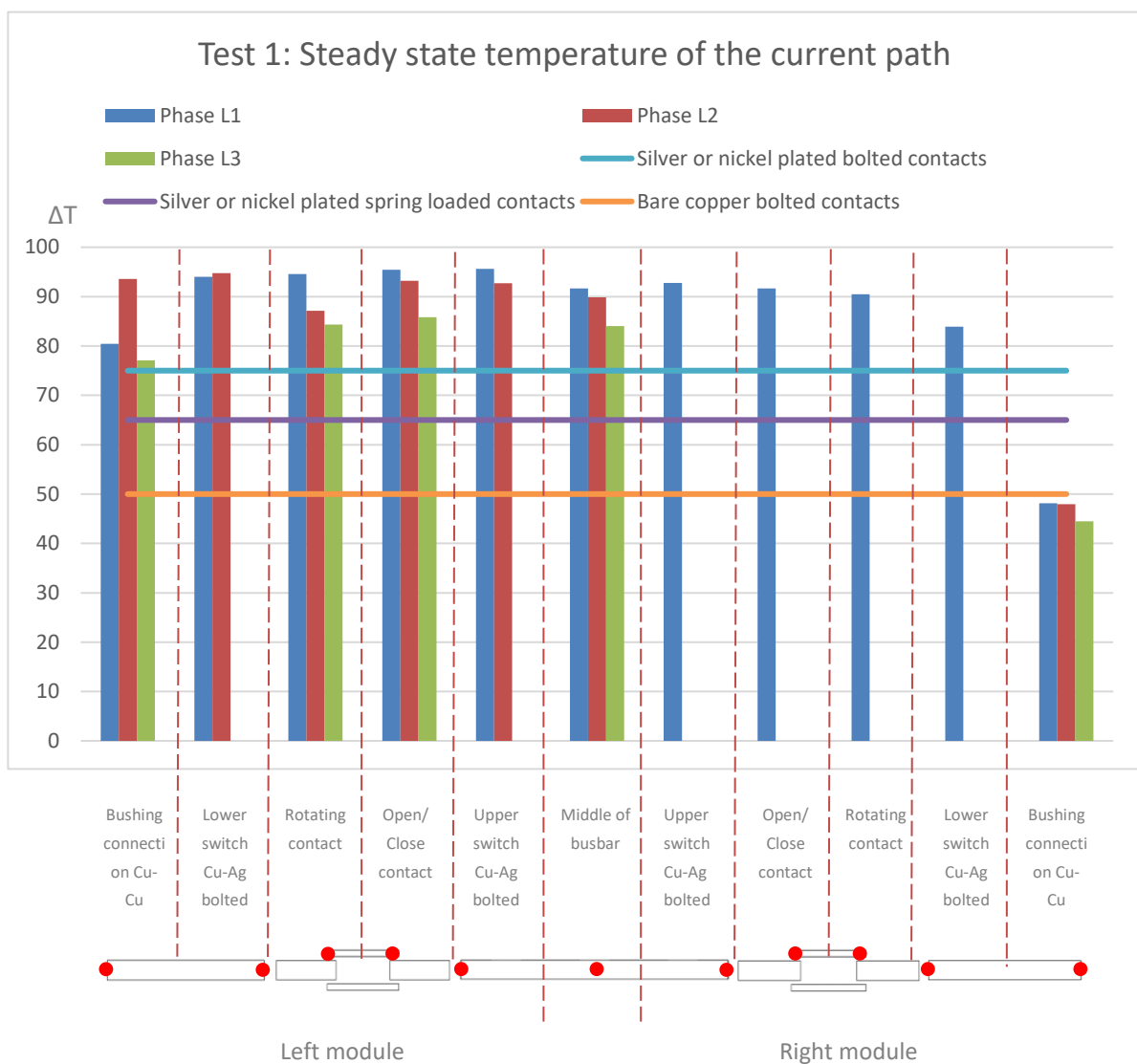


Figure 6.3 – Steady state temperature rise of the measuring points along the current path in the RMU enclosure for test 1

There is just a minor difference between the temperature of the bolted contacts and the rotating and open/close contacts. As mentioned earlier, the temperature read by the thermocouples at the bolted contacts are located closer to the actual points in contacts with each other than the thermocouples at the rotating contacts and open/close contacts. There is a possibility that the temperatures read by the thermocouples at the rotating contacts and open/close contacts are lower than the actual temperature of the contact point, since the thermocouples are mounted a few millimeters away from the contacts.

There is a large difference in the temperature of the bolted Cu-Cu bushing connections in the right module to the bolted Cu-Cu bushing connections in the left module. In the right module the power cables from the current injector are mounted, and there is a possibility that heat is transferred by the cables. On the left module the bushings are short-circuited.

The temperatures of the cables were checked when steady state was reached, and the difference between the measuring points was less than 5°C. The measuring points were located 1 meter and 2 meters away from the bushing connection. In Appendix C, the exact temperatures of these measuring points are given.

6.3.2 Measured steady state temperature of test 2: nonmagnetic bolts

Figure 6.4 shows a plot of the steady state temperature of the measuring points along the current path for test 2. The axes for Figure 6.4 are the same as for test 1 in Figure 6.3. The x-axis is given as the switch, the y-axis is the temperature rise.

The horizontal lines represent the maximum temperature rise limits for spring loaded and bolted contacts given by IEC [6].

Table 6.5 shows the steady state temperatures of the additional thermocouples mounted near the upper switch connection on phase L1 and L2 as presented in chapter 4.1.1.

Table 6.5 – Steady state temperature for additional thermocouples in test 2

Phase	Position	Module	[ΔT] [°C]
L1	Near upper switch Cu-Ag bolted connection	Right	88,0
L2	Near upper switch Cu-Ag bolted connection	Right	78,8

Temperature rise

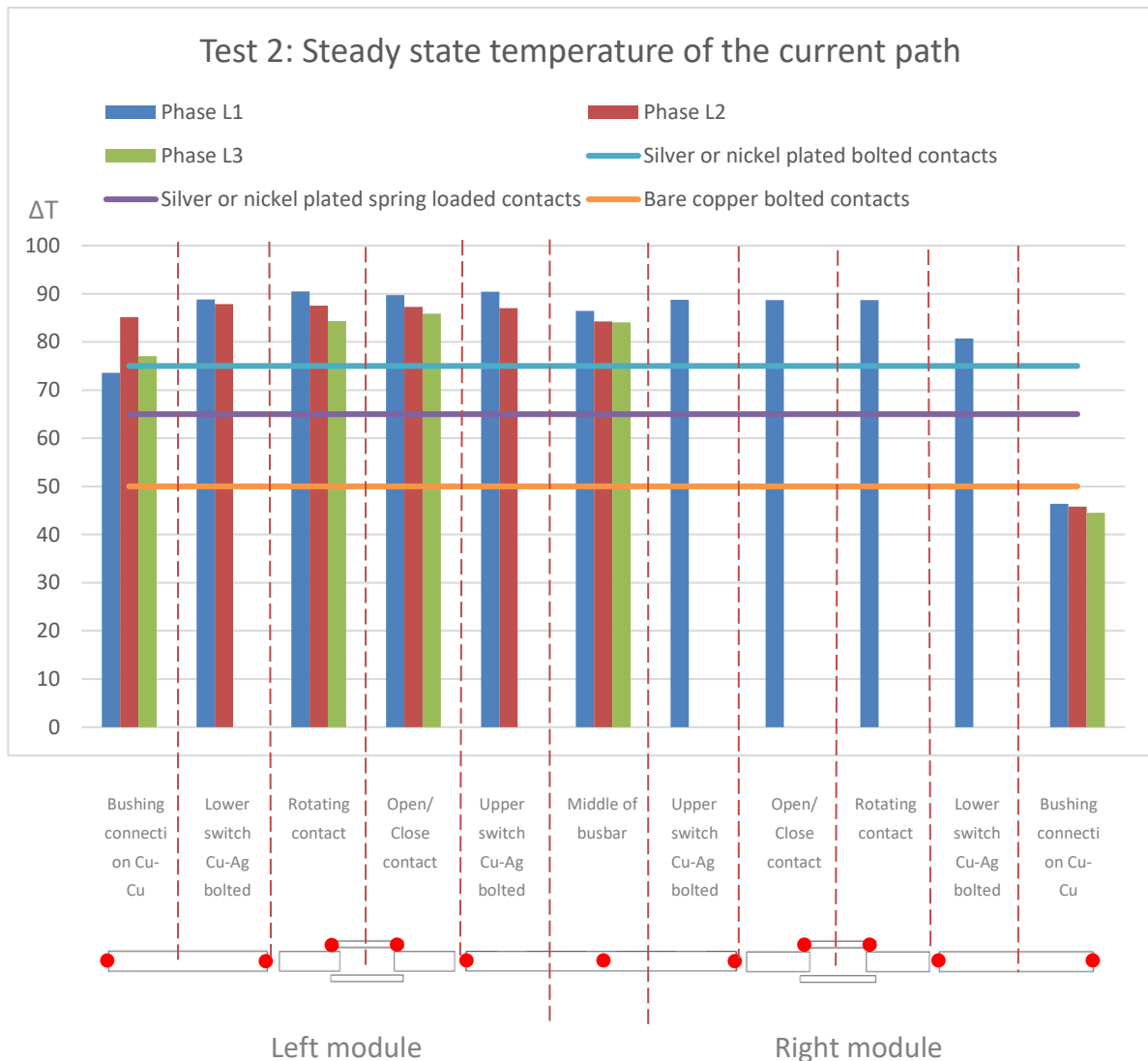


Figure 6.4 – Steady state temperature rise of measuring points along the current path in the RMU enclosure for test 2

The temperatures in Figure 6.4 for test 2 shows the same tendencies as for test 1. The steady state temperatures are however a little lower in test 2, the reduced power loss of about 5W is not enough to explain a reduction of 2-10% for almost all measuring points.

The thermocouples near the upper bolted Cu-Ag switch connection, is only a barely lower than the thermocouple mounted beneath the washer in phase L1.

Table 6.6 shows the exact result from test 1 and test 2 listed.

Table 6.6 – Steady state temperatures of the measuring point along the current path for test 1 and test 2

Sensor	Position and description	Module	Test 1	Test 2
			ΔT [°C]	ΔT [°C]
Phase L1				
1	Bushing connection Cu-Cu bolted connection	Left	80,46	73,60
2	Lower switch connection Cu-Silver bolted connection	Left	94,02	88,80
3	Rotating contact	Left	94,59	90,46
4	Open/Close contact	Left	95,46	89,73
5	Upper switch connection Cu-Silver bolted connection	Left	95,64	90,39
6	Middle of busbar		91,66	86,47
7	Upper switch connection Cu-Silver bolted connection	Right	92,75	88,77
8	Open/Close contact	Right	91,63	88,70
9	Rotating contact	Right	90,47	88,68
10	Lower switch connection Cu-Silver bolted connection	Right	83,90	80,70
11	Bushing connection Cu-Cu bolted connection	Right	48,15	46,38
Phase L2				
12	Bushing connection Cu-Cu bolted connection	Left	93,60	85,15
13	Lower switch connection Cu-Silver bolted connection	Left	94,72	87,82
14	Rotating contact	Left	87,12	87,54
15	Open/Close contact	Left	93,19	87,30
16	Upper switch connection Cu-Silver bolted connection	Left	92,73	87,01
17	Middle of busbar		89,88	84,27
29	Bushing connection Cu-Cu bolted connection	Right	47,92	45,79
Phase L3				
31	Bushing connection Cu-Cu bolted connection	Left	83,04	77,06
18	Rotating contact	Left	90,63	84,33
19	Open/Close contact	Left	90,85	85,85
32	Middle of busbar		88,48	84,04
30	Bushing connection Cu-Cu bolted connection	Right	67,62	45,32

All the steady state temperatures of the current path are given in Appendix H.

6.4 Influence of magnetic bolts and washers

In this section, the changes in the steady state temperature is discussed when the bolts and washers made of magnetic material are replaced with bolts and washers made of nonmagnetic material.

Table 6.7 shows the temperature reduction in the bolted Cu-Cu bushings connections. The reduction is biggest in the right module, this is could be because the resistance of the bushing connections in the right module are probably reduced compared to the resistance of the bushing connections in the left module. (The bolts in the bushing connections in right module were fastened a bit more than the bolts in the left bushing connections)

Table 6.7 – Steady state temperature of the bushing connections Cu-Cu bolted connections

Sensor	Phase	Module	Percentage reduction temperature in the bushing connections
1	L1	Right	8,5%
12	L2	Right	9,0 %
31	L3	Right	7,2 %
11	L1	Left	3,7%
29	L2	Left	4,4 %
30	L3	Left	1,8 %

6.4.1 Air inside RMU enclosure

The steady state air temperature was reduced significantly when the magnetic bolts and washers (test 1) was replaced with nonmagnetic bolts and washers (test 2). According to Table 6.4, the temperature of the inside air near the bottom of the enclosure is reduced with 27,5%, and the temperature of the air in the mid-height of the enclosure is reduces with 17,2%.

The resistance and corresponding power loss reduction from test 1 to test 2 are barely 5W, and this is not enough to contribute to such a reduction in the air temperature. This result implies that the magnetic bolts contributed with an extra heat input of significant size. When the switchgear was connected to the AC power source, eddy currents caused by the changing magnetic field in the conductors probably contributed to a power loss within the bolts. The extra power loss contributed to the heat transfer to the surroundings.

6.4.2 Conductors and switches

Figure 6.5 shows the steady state temperatures for test 1 and test 2 of the switches in the left module for phase L1 and L2. For better visualization of the temperature trend, the point of congelation has been moved to 80°C in Figure 6.5.

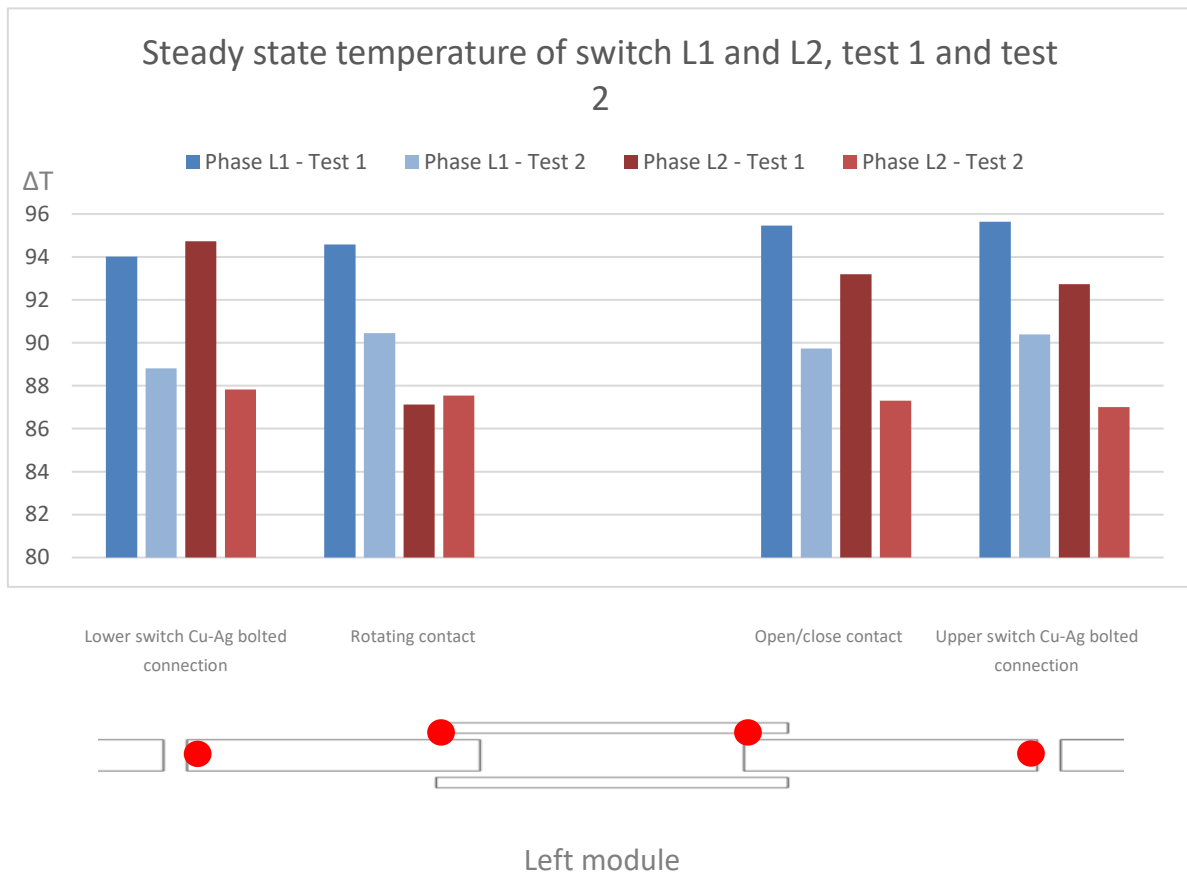


Figure 6.5 – Graphical illustration of the steady state temperature rise of parts of the current path with magnetic and nonmagnetic bolts and washers

Figure 6.5 shows a small temperature decrease from test 1 to test 2 for almost every measurement point of the switch in phase L1 and L2 in the left module, except for the rotating contact in phase L2. As discussed earlier, the contact resistances had large variations for the rotating contacts and the open/close contacts. There is a possibility that the contact resistances changed when the bolts were replaced, due to their sensitivity to different positions. The contact resistances were measured before the temperature rise test 2 was conducted, and the resistances were in the same order as previous results. Small deviations from test 1 is still a possibility and could therefore affect the temperatures.

The temperatures of the switch in phase L1 are however significantly lower in test 2. This result also imply that the material of the bolts does impact the steady state temperature along the current path as well as the air temperature. The steady state air temperature was reduced more than the temperature of the conductors, with lower temperature of the conductors the heat

Temperature rise

transfer to air could be a little lower and therefore also contribute to a lower steady state air temperature.

6.5 Influence of mounting mechanisms of the thermocouples

In this section, the influence of the mounting mechanism of the thermocouples are discussed.

In test 2, an extra thermocouple where mounted on phase L1 as described in Chapter 4.1.3. In similar experiments, the thermocouples are mounted with strips and tape as near the contacts as possible. When the thermocouples are mounted beneath the washers, the temperature is read closer to the contacts and could be the reason the temperatures are higher than in the previous results.

Table 6.8 shows the temperature of the thermocouple mounted beneath the washer and the thermocouple mounted near the bolted connection.

Table 6.8 – Temperature rise of the test 2 for the upper switch Cu-Ag bolted connections for phase L1

Sensor	Position and description	Phase	Module	Test 2 [°C]
5	Upper switch connection Cu-Ag bolted connection	L1	Right	88,77
	<i>Near upper switch Cu-Ag bolted connection</i>	<i>L1</i>	<i>Right</i>	<i>88,00</i>

The temperatures of thermocouples located near the upper switch bolted connection are barely lower than the thermocouple located beneath the washer. The difference is in fact low enough to be neglected. The low difference imply that the mounting mechanism does not impact the read temperature of the bolted connections.

6.6 Discussions

In this section, the results from the temperature measurements are discussed.

6.6.1 IEC temperature limits

The first thing that is noticeable from the steady state temperature from test 1 and test 2 in Figure 6.3 and Figure 6.4 is that the steady state temperatures are higher than limits set by IEC. The temperature rise of the Cu-Cu bolted contacts should not exceed 50°C, the Cu-Ag bolted contacts should not exceed 75°C and the rotating contact and open/close contacts should not exceed 65°C. The test device was not meant to satisfy these limits, and this will not be discussed further.

6.6.2 Steady state air temperature of the RMU enclosure

Table 6.9 shows the measured and estimated values of the air temperature inside the RMU enclosure. The estimated temperature in mid-height are higher than the measured temperature, while the estimated temperatures in the top-height of the enclosure are lower than the measured temperatures.

Table 6.9 – Summarized steady state air temperature inside RMU enclosure

	$\Delta t_{1,0}$ [°C]		$\Delta t_{0,5}$ [°C]	
	Measured	Estimated	Measured	Estimated
Test 1	38,6	35	24,9	27
Test 2	34,3	34	20,7	26

The empirical method from IEC is based on parameters that assume a uniformly heat generation and does not include the location of the conductors. This is contributing to an error in the estimated value. The method strictly dependent on choosing proper factors as well and reading the graphs in the IEC report correctly [7]. The estimated temperatures should therefore be used more as a guidance.

Overall, the measures temperatures are in the same order as the estimated. The tendencies are the same, where the temperatures of test 1 are barely higher than the temperatures of test 2. This is because the power loss is slightly lower for test 2.

The measured air temperature in the mid-height of the test device is lower than the temperature found in the report “Heat transfer mechanisms in MV load break switches”, this could be due to less heat generation in the bottom of the test device [14]. The main parts of the current paths are located in the upper part of the enclosure, and the heat generation is therefore larger there than in the middle and bottom of the enclosure. The temperature near the top-height of the enclosure is about 13-14°C higher than in the mid-height.

6.6.3 Steady state temperature of the current path

The steady state temperatures of test 1 with magnetic bolts in phase L1 are higher than the steady state temperatures of phase L2 and L3. Phase L1 has a higher total resistance, and the higher temperature rise matches this finding.

There are only a few degrees difference between the rotating contact and the open/close contact. The interesting thing is that for all three phases in the left module the temperature of the open/close contact is in fact higher than the rotating contact. This is unexpected based on the results from the contact resistance measurements, where the rotating contact resistance were larger than the resistance of the open/close contact.

The thermocouples belonging to the rotating- and open/close contacts are located on the visible part of the outer contact, as shown in chapter 4.1.1. The temperature of the exact contact points in the rotating contact could therefore be some higher than the measured temperature. This was investigated in chapter 6.5 for the upper bolted contact in the right module, and the temperature difference between the thermocouple located beneath the bolt and the thermocouple near the bolt was very small. This implies that the mounting should not impact the temperature of the rotating contact in a great extent, but it is important to emphasize that this was concerning a bolted contact. The temperature read by the thermocouple located near the open/close or rotating contact could be lower than the actual temperature of the contact.

Figure 6.6 shows the temperatures of test 1 and test 2 for phase L1. The x-axis is given as the current path, and the y-axis is the temperature rise.

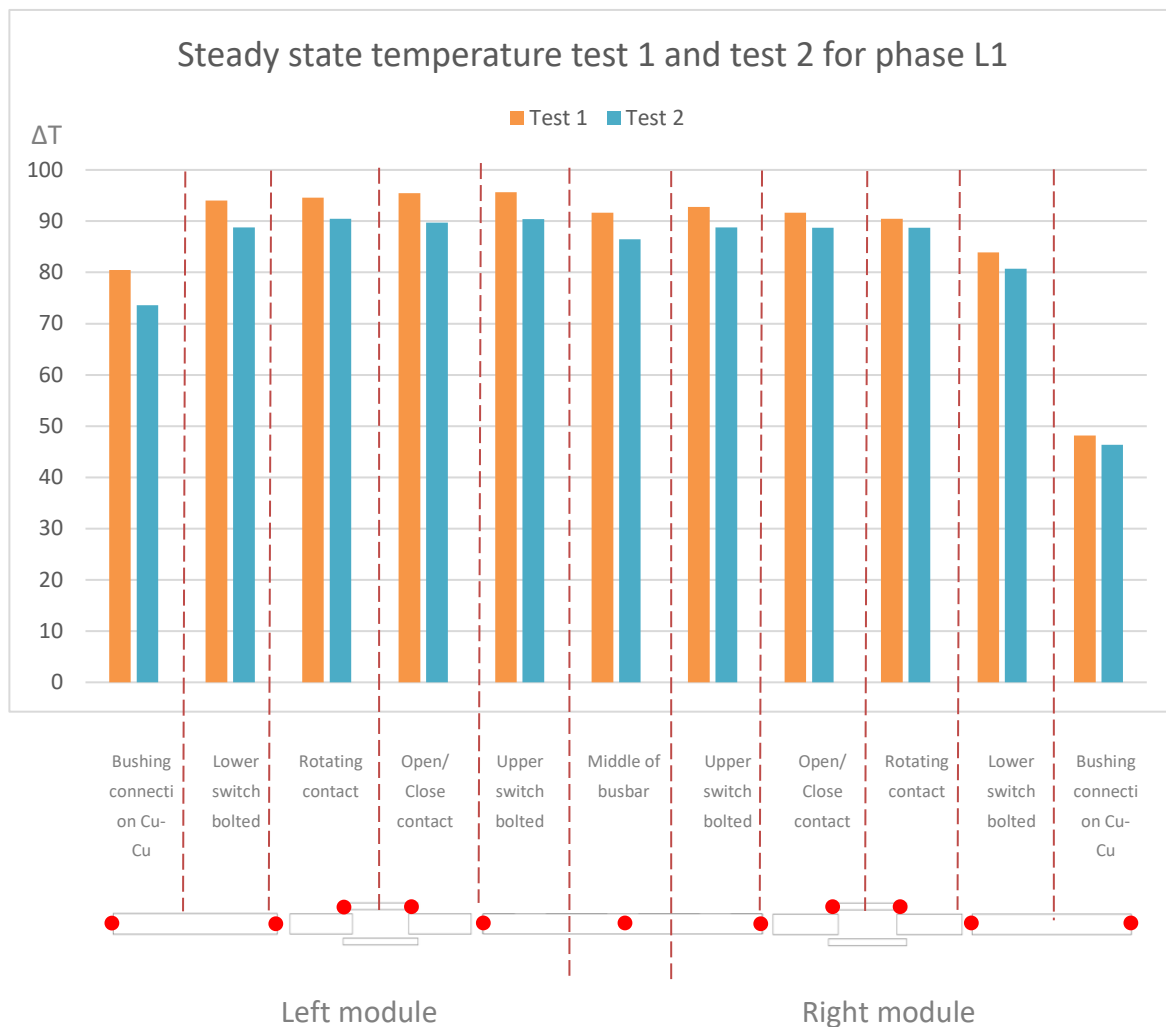


Figure 6.6 – Comparison between steady state temperatures of phase L1 in test 1 and test 2

Figure 6.6 clearly shows similar trends in both test for phase L1. The temperatures between the lower Cu-Ag connection from the left module to the right module of test 2 are however more uniform than for test 1. The differences between the left and right module are lower for test 2.

The temperature rise is reduced with an average for all measurements of about 5% when the magnetic bolts and washers is replaced with nonmagnetic ones. There was almost no change in the power loss from test 1 to test 2, and the small difference is not enough to explain the temperatures reduction alone. As already discussed, the magnetic bolts and washers probably contributed with an extra heat input due to induced power in the magnetic material.

The mounting of the thermocouples shows a very small change in the temperature. The difference between mounting the thermocouple with strips and tape and beneath the washers are negligible.

The temperatures of the current path in phase L1 is higher than the results in similar experiments. The maximum temperature rise occurring on the knife switch in the test device is

Temperature rise

about 95°C. In the report “Heat transfer mechanisms in MV load break switches”, the temperature rise of a knife switch reaches a maximum temperature of about 78°C [14]. In the report “Power loss and temperature rise in a four-module switchgear” the temperature rise of the switch is about 75°C [13].

In the test device, there are less components involved inside the enclosure than for a real switchgear. This is briefly discussed in Chapter 3. It was implied that this simplified design of the test device could affect the heat transportation within the enclosure. The relatively high temperatures of the current path imply that the temperatures are affected by the lack of supportive components, such as mechanism for operating the switchgear and stabilizing equipment. These additional components contribute to transporting the generated heat, i.e. the cooling surfaces appearing are larger.

7 Heat transfer coefficient

In this chapter, the heat transfer coefficient for phase L1 is calculated and discussed.

7.1 Calculation of the heat transfer coefficient

In order to calculate the heat transfer coefficient, some simplifications are made. Figure 7.1 shows a sketch of how the current path is divided to perform the calculations. The heat transfer coefficients are only calculated for phase L1. The formula needed to calculate the heat transfer coefficient is shown in Equation (2.5).

The temperatures used to find the resulting ΔT between conductor and air needed in Equation (2.5), are the temperature difference between the two ending points of each conductor, ΔT_{con} and temperature difference between top/bottom and middle air ΔT_{air} . The temperatures are all taken from test 1 with magnetic bolts.

The surface area U is based on assumption on which surfaces of the conductor are “facing” the surroundings. The inner surfaces of the knife blades are excluded for the switch. The surface of the sides of the conductors are assumed to be so small that they are excluded. The power loss in the parts are estimated from the resistance during reference temperature.

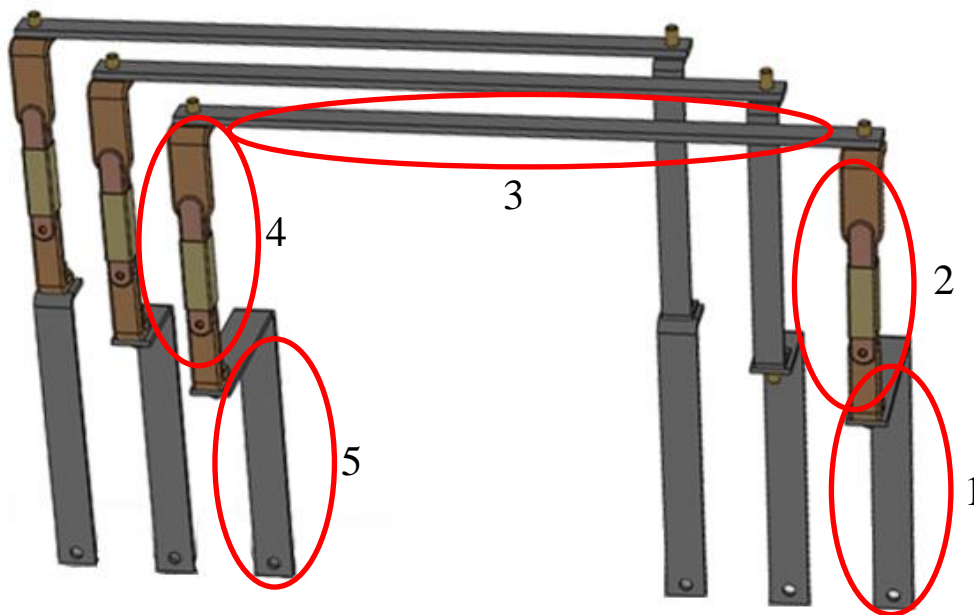


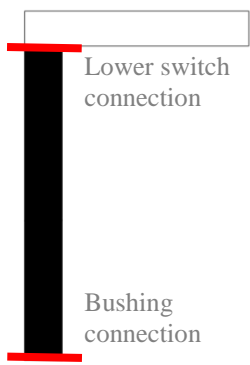
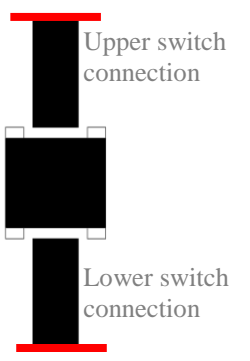
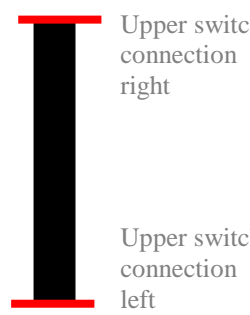
Figure 7.1 – Sketch of the individual parts to calculate heat transfer coefficients

Table 7.1 shows the surface area and resulting heat transfer coefficient for the individual parts as shown in Figure 7.1. The following parameters are given in Table 7.1:

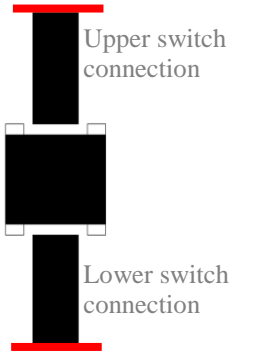
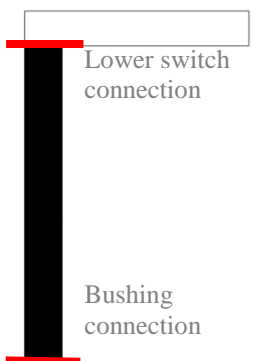
U = Surface area [m^2]

h = Heat transfer coefficient [$\frac{\text{W}}{\text{m}^2 \cdot ^\circ\text{C}}$]

Table 7.1 – Calculation of the heat transfer coefficient

Part:	Sketch:	Explanation:	U	h
			[m^2]	$[\frac{\text{W}}{\text{m}^2 \cdot ^\circ\text{C}}]$
1		<p>From bushing connection to height of lower switch connection</p> <p>Right module</p>	0,0276	10,2
2		<p>From and including upper switch connection to and including lower switch connection</p> <p>Right module</p>	0,0053	42,0
3		<p>From upper switch connection right module to upper switch connection</p> <p>Left module</p>	0,052	8,5

Heat transfer coefficient

4		<p>From and including upper switch connection to and including lower switch connection</p> <p>Left module</p>	0,0053	40,2
5		<p>From bushing connection to height of lower switch connection</p> <p>Left module</p>	0,0276	6,8

The average heat transfer coefficient for the current path is 21,5 W/(m²°C). In appendix H, the excel sheets used for calculation is given.

7.2 Discussion

Table 7.1 shows a large variation between the coefficients of the switch and the conductor bars. The coefficients are based on several assumptions and estimations, the values do therefore contain some uncertainties.

In the report “Thermal design of future medium voltage switchgear”, the heat transfer coefficient was found to be 12 W/m²°C for a knife switch [9]. This is lower than the heat transfer coefficient for the switches of 40-42 W/m²°C the test device. The large heat transfer coefficient is probably due to the large temperature difference between the air and the conductive parts. This again, could be due to the lack of supportive components that helps transporting the generated heat of the conductors.

8 Conclusion

In this chapter, the conclusion of the results and discussion is presented.

For the test device to be realistic, the behavior of the test device should be similar to a real switchgear.

The total resistance of the test device is a little less than ideally, resulting in a power loss that is in the lower range as well. The contact resistances of the rotating contact and open/close contacts showed large variations and was somewhat higher than results from previous experiments. The contacts of the switch appear to be sensitive to changes of the knife blade position. For the test device to be realistic, the variation in the contact resistances of the rotating contact and open/close contact should be reduced. The relation between bulk resistance and contact resistance of the test device is in the same order as previous results.

The total resistance and power loss was impacted in a small extent by replacing the magnetic bolts and washers with nonmagnetic ones. The steady state temperature was however lowered with a few degrees when the bolts and washers were replaced with nonmagnetic ones, this implies that there was an extra heat input added by induced voltage in the material.

Even though the power loss is a little lower than ideally, the temperature rise of the conductors are exceeding the IEC limits by great extent in both the tests. The lack of components involved for supportive purposes inside the enclosure implies that the heat transportation is influenced. The heat transportation appears to be lower for the test device, resulting in a higher temperature of the conductive parts.

The main parts of the current path are in addition located in the upper section of the RMU enclosure, leaving the bottom section to have less heat generation. In a real compact switchgear there are several more components involved than in the test device, and the enclosure is more uniformly filled with parts.

Overall, the test device is somewhat realistic. But the relatively high temperatures of the current path are a concern. The temperatures of the current path are a lot higher than the temperatures of similar switchgears, even though the power loss of the test device is less than the power loss in the similar switchgear. The temperature of the current path should be reduced for the test device to be used as a guidance for simulations tools,.

References

- [1] W. Rondeel, "Physics in Electrical Engineering Lectures, EPE2416," University College of Southeast Norway, Porsgrunn, 2018.
- [2] Society of electrical and electronics engineers, "Electrical & Electronics," 30 May 2018. [Online]. Available: <https://electricalstudyportal.blogspot.no/2015/05/power-system-topic-sai-saikumar-jn.html>. [Accessed 03 May 2018].
- [3] Wikipedia, "Switchgear," 02 may 2018. [Online]. Available: <https://en.wikipedia.org/wiki/Switchgear>. [Accessed 03 May 2018].
- [4] Google, "IndiaMart," [Online]. Available: https://www.google.com/search?safe=off&rlz=1C1GGRV_enNO792NO792&biw=958&bih=1074&tbm=isch&sa=1&ei=eZH0WqS2LISqsgH-m6OQCw&q=switchgear+abb+12+kV&oq=switchgear+abb+12+kV&gs_l=img.3...211178.212169.0.212446.6.6.0.0.0.62.331.6.6.0...0...1c.1.64.img..0.2.11. [Accessed 03 May 2018].
- [5] Wikipedia, "Wikipedia," 31 December 2017. [Online]. Available: https://en.wikipedia.org/wiki/Electrical_contacts. [Accessed 09 Januar 2018].
- [6] International Electrotechnical Comite, "62271-1," Norsk Elektrotekniske Komite, 2011.
- [7] Electrical Engineering Portal, "Electrical Engineering Portal," [Online]. Available: <http://electrical-engineering-portal.com/5-copper-busbar-jointing-methods>. [Accessed 02 April 2018].
- [8] ABB, A.Hoppner, "ABB Switchgear manual," Cornelsen Verlag, Berlin, 1999.
- [9] E. Fjeld, W. Rondeel, K. Vaagsaether, M. Saxegaard, P. Skryten and E. Attar, "Thermal design of future medium voltage switchgear," 15-18 Juni 2015. [Online]. Available: http://cired.net/publications/cired2015/papers/CIRED2015_1090_final.pdf. [Accessed 12 Februar 2018].
- [10] International Electrotechnical Commision, "A method of temperature-rise verification of low-voltage switchgear and controlgear assemblies by calculation NEK IEC TR 60890:2014," Norsk Elektroteknisk komite, 2014.
- [11] AUTEK, "Temperatur," AUTEK, [Online]. Available: <http://autek.no/wp-content/uploads/temperaturkatalog.pdf>. [Accessed 03 03 2018].
- [12] Gossen Metrawatt, "TRMS System Multimeter," [Online]. Available: https://www.elit.no/media/catalog/product/d/b/db_gb_7.pdf. [Accessed 16 April 2018].

- [13] A. Chynchenko, D. K. Kvam and S. Øygarden, "Power loss and temperature rise in a four-module switchgear," USN, Porsgrunn, 2016.
- [14] S. Øygarden, "Heat transfer mechanisms in MV load break switches," USN, Porsgrunn, 2017.
- [15] E. Fjeld, W. Rondeel, S. T. Hagen and M. Saxegaard, "Estimating the temperature rise of load break switch contacts in enclosed MV switchgear," CIRED, Glasgow, 2017.

Appendices

Appendix A: Problem description

Appendix B: Positions of the thermocouples

Appendix C: Steady state temperature of other temperatures of interest

Appendix D: Calculations of bulk resistances

Appendix E: Measurements of the contact resistances

Appendix F: Estimation of bulk resistance during steady state temperature

Appendix G: Steady state air temperatures

Appendix H: Steady state temperatures of the current path

Appendix I: Heat transfer calculations

Appendix A: Problem description

HSN University College
of Southeast Norway
Faculty of Technology, Natural Sciences and Maritime Sciences, Campus Porsgrunn

FMH606 Master's Thesis

Title: Power loss measurements of MV switchgear for Cigré-working group

HSN supervisor: Elin Fjeld / Wilhelm Rondeel

External partner: ABB AS

Task background:

Cigré (International Council on Large Electric Systems) is an association where experts from all around the world work together in working groups to improve electric power systems. Simulation technologies have an increasing role in the development and verifying the performance of equipment, and working group A3.36 is studying to what degree simulations can be used to predict the steady state temperature rise of MV and HV switchgear. Simulation experts of the working group (from different companies) will use their different simulation tools and experience to simulate the temperature rise of switchgear. The results will be compared to each other, and to experimental results. The experimental tests on the MV switchgear will be performed at the University College of Southeast Norway.

Task description:

A test device is being made, and the master student should work together to finalize/assemble the test device. The test device should have a realistic design, power input and number of contacts/connections.

The student should then:

- Calculate theoretical bulk resistance.
- Measure bulk and contact resistance.
- Estimate and measure resistance during full load warm conditions.
- Measure the temperature rise at full load conditions. Repeat the experiments with an adjusted load if the temperature rise is too far from the relevant IEC limits.
- Calculate and measure total power loss.

The results will be provided to the Cigré Working group.

Student category: EPE students

Practical arrangements:

Equipment for performing temperature rise tests is available at USN.

Signatures:

Student (date and signature): 15/1-18 Sandra Helland

Supervisor (date and signature): 15/1-18 Elin Fjeld

Address: Kjølnes ring 56, NO-3918 Porsgrunn, Norway. Phone: 35 57 50 00. Fax: 35 55 75 47.

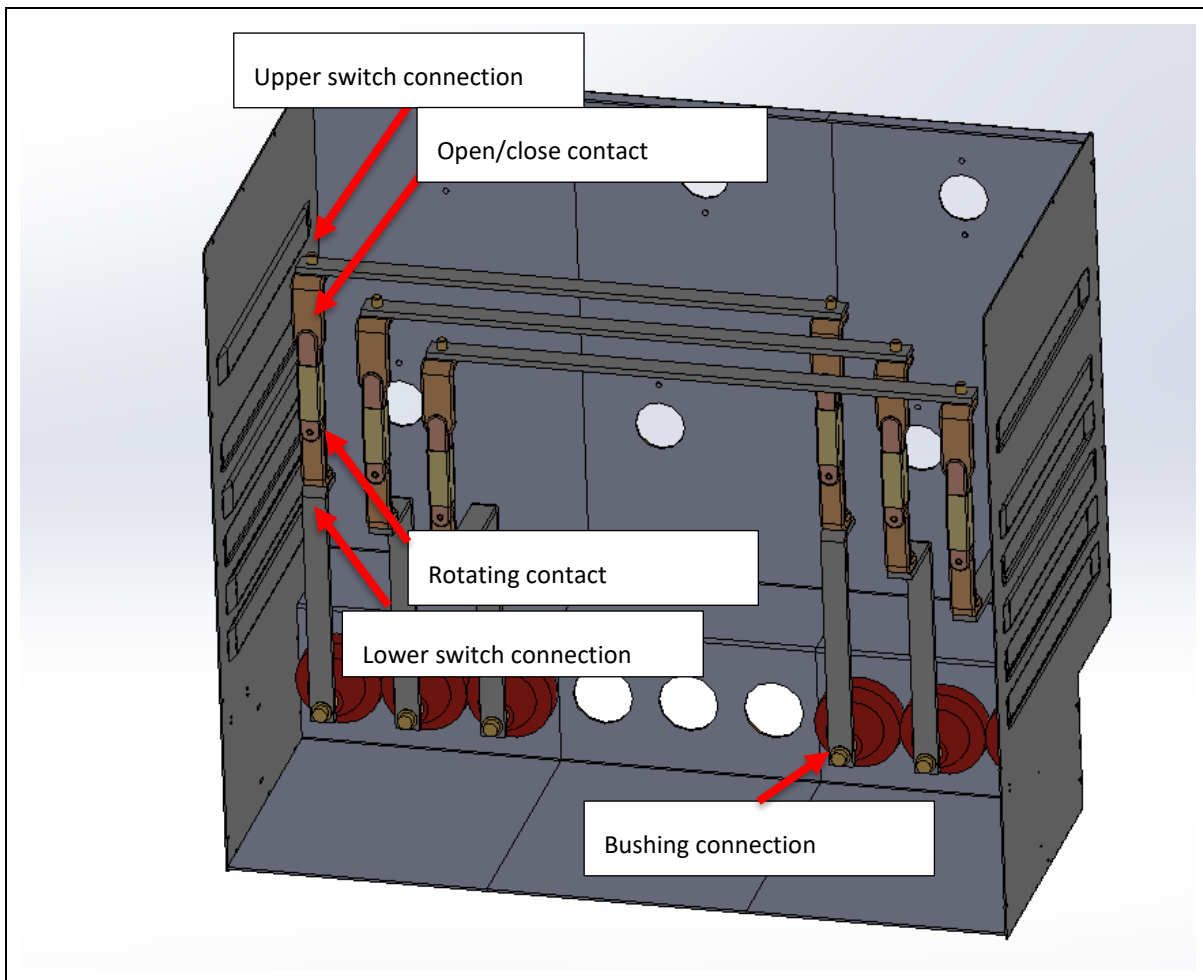
Appendix B: Positions of thermocouples

Position of thermocouples of the current path and air:


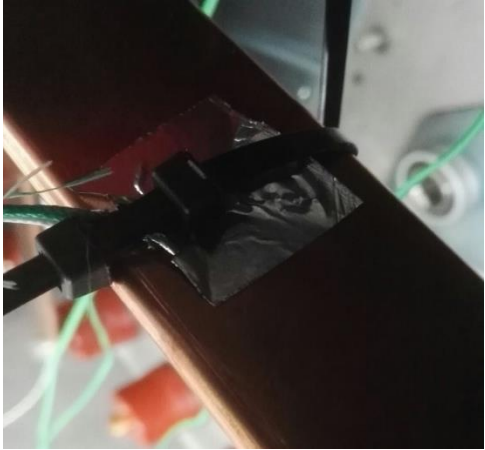

Sensor no	Position and description	Phase	Module
1	Bushing connection Cu-Cu bolted connection	L1	Left
2	Lower switch connection Cu-Ag bolted connection	L1	Left
3	Rotating contact	L1	Left
4	Open/Close contact	L1	Left
5	Upper switch connection Cu-Ag bolted connection	L1	Left
6	Middle of busbar	L1	
-	Near upper switch connection Cu-Ag bolted	L1	Right
7	Upper switch connection Cu-Ag bolted connection	L1	Right
8	Open/Close contact	L1	Right
9	Rotating contact	L1	Right
10	Lower switch connection Cu-Ag bolted connection	L1	Right
11	Bushing connection Cu-Cu bolted connection	L1	Right
12	Bushing connection Cu-Cu bolted connection	L2	Left
13	Lower switch connection Cu-Ag bolted connection	L2	Left
14	Rotating contact	L2	Left
15	Open/Close contact	L2	Left
16	Upper switch connection Cu-Ag bolted connection	L2	Left
17	Middle of busbar	L2	
-	Near upper switch connection Cu-Ag bolted	L2	Right
18	Rotating contact	L3	Left
19	Open/Close contact	L3	Left
20	Inside air Near top of compartment		
21	Inside air Middle of compartment		
22	Inside air Near bottom of compartment		
29	Bushing connection Cu-Cu bolted connection	L2	Right
30	Bushing connection Cu-Cu bolted connection	L3	Right
31	Bushing connection Cu-Cu bolted connection	L3	Left
32	Middle of busbar	L3	
	Room temperature		

Thermocouples requested by the working group:

Sensor no	Position and description
23	Middle of inside side wall
24	Middle of inside back wall
25	Middle of inside front wall
26	Middle of inside top surface
27	Middle of outside side wall
28	Middle of outside front wall



Appendices

	<p>Rotating contact</p>
	<p>Middle of busbar</p>
	<p>Bolt below switch</p>

	<p>Bolt bushing connection</p>
	<p>Outside side wall</p>
	<p>Inside side wall</p>
	<p>Air near top (47 mm from top)</p>

Appendices



Air middle (415 mm from top)



Air near bottom (775 from top)

Appendix C: Steady state temperature of other temperatures of interest

Temperature of the walls:

Sensor	Position and description	Test 1		Test 2	
		T_{abs} [°C]	ΔT [°C]	T_{abs} [°C]	ΔT [°C]
23	Middle of inside side wall	40,19	17,89	38,49	16,59
24	Middle of inside back wall	43,66	21,36	39,68	17,78
25	Middle of inside front wall	36,25	13,95	34,61	12,71
26	Middle of inside top surface	41,46	19,16	40,73	18,83
27	Middle of outside side wall	33,26	10,96	32,73	10,83
28	Middle of outside front wall	34,90	12,60	31,99	10,09

Temperature of the cables:

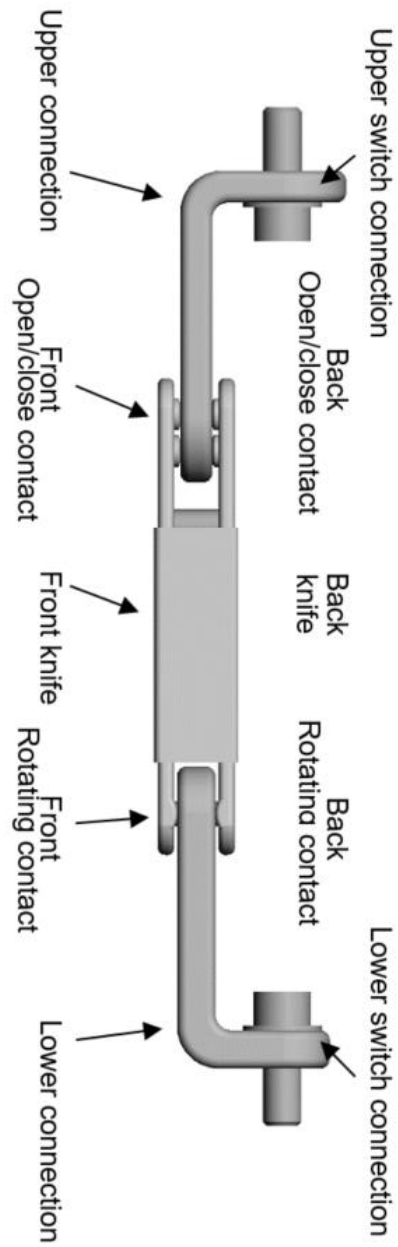
Phase	Position of thermocouple on cable	Test 1		Test 2	
		T_{abs} [°C]	ΔT [°C]	T_{abs} [°C]	ΔT [°C]
L1					
	1 meter	47,10	24,80	46,10	23,50
	2 meter	45,90	23,60	45,90	23,30
L2					
	1 meter	48,00	25,70	47,80	25,20
	2 meter	46,10	23,80	46,70	24,10
L3					
	1 meter	47,30	25,00	47,10	24,50
	2 meter	46,30	24,00	46,30	23,70

Appendix D: Calculation of cold bulk resistances

Specific resistance $\rho = 0,01786 \Omega * \frac{mm^2}{m}$, Temperature coefficient $\alpha = 3,92 * 10^{-3}$

Replacement bar			
Total length	330	mm	
Width	40	mm	
Depth	6	mm	
Cross-section area	240,00	mm ²	
Bulk resistance	24,26	μΩ	
Busbar			
Total Length	650	m	
Width	40,00	mm	
Depth	6,00	mm	
Cross-section area	240,00	mm ²	
Bulk Resistance	47,50	μΩ	
Connection bar L1			
Total Length	470	m	
Width	40,00	mm	
Depth	6,00	mm	
Cross-section area	240,00	mm ²	
Bulk Resistance	34,20	μΩ	
Connection Bar L2			
Total length	370	m	
Width	40,00	mm	
Depth	6,00	mm	
Cross-section area	240,00	mm ²	
Bulk Resistance	26,97	μΩ	
Connection Bar L3			
Total length	330	m	
Width	40,00	mm	
Depth	6,00	mm	
Cross-section area	240,00	mm ²	
Bulk Resistance	24,30	μΩ	

Switch			
Upper switch connection			
length	30	mm	
width	27	mm	
depth	9	mm	
Cross section area	243	mm ²	
Bulk resistance	2,2	μΩ	
Upper connection			
length	80	mm	
width	27	mm	
depth	9	mm	
Cross section area	243	mm ²	
Bulk resistance	5,9	μΩ	
Front/Back knife			
length	120	mm	
width	25	mm	
depth	4	mm	
Cross section area	100	mm ²	
Bulk resistance	21,4	μΩ	
Lower connection			
length	100	mm	
width	37	mm	
depth	7	mm	
Cross section area	259	mm ²	
Bulk resistance	6,9	μΩ	
Lower switch connection			
length	30	mm	
width	37	mm	
depth	7	mm	
Cross section area	259	mm ²	
Bulk resistance	2,1	μΩ	
Total bulk resistance R_{B-Switch}	38,5	μΩ	



Appendix E: Contact resistance measurements small enclosure

	Switch L1 Right				Switch L1 Left		
	Test 1	Test 2	Test 3		Test 1	Test 2	Test 3
	[$\mu\Omega$]	[$\mu\Omega$]	[$\mu\Omega$]		[$\mu\Omega$]	[$\mu\Omega$]	[$\mu\Omega$]
Upper contact	1,3	0,9	1,0	Upper contact	1,0	1,2	1,0
Upper connection	7,5	7,1	7,0	Upper connection	5,7	6,9	7,1
Open/Close contact				Open/Close contact			
Front	25,1	16,9	15,0	Front	13,8	18,1	14,6
Back	27,1	17,0	15,5	Back	14,2	19,2	14,1
Knife				Knife			
Front	17,4	12,6	13,8	Front	15,4	12,6	13,8
Back	18,6	16,8	14,8	Back	16,2	16,8	14,8
Rotating contact				Rotating contact			
Front	20,1	20,6	16,9	Front	19,1	17,8	18,6
Back	23,4	20,1	16,7	Back	21,1	18,3	18,9
Lower connection	2,8	2,7	4,7	Lower connection	4,9	4,2	4,3
Lower contact	3,0	2,2	2,0	Lower contact	1,8	2,1	1,9
	Switch L2 Left				Switch L3 Left		
	Test 1	Test 2	Test 3		Test 1	Test 2	Test 3
	[$\mu\Omega$]	[$\mu\Omega$]	[$\mu\Omega$]		[$\mu\Omega$]	[$\mu\Omega$]	[$\mu\Omega$]
Upper contact	2,0	3,23	2,0	Upper contact	2,3	1,0	1,5
Upper connection	3,4	4,5	5,1	Upper connection	7,8	5,9	6,8
Open/Close contact				Open/Close contact			
Front	14,0	14,4	13,8	Front	15,2	17,4	13,7
Back	17,6	16,2	15,7	Back	18,8	15,1	13,8
Knife				Knife			
Front	15,2	19,0	17,6	Front	18,2	12,6	13,8
Back	29,6	18,2	20,8	Back	17,4	16,8	14,8
Rotating contact				Rotating contact			
Front	31,4	26,2	38,9	Front	20,1	20,6	16,9
Back	42,7	36,6	34,0	Back	23,4	20,1	16,7
Lower connection	5,7	5,1	5,4	Lower connection	2,8	2,7	4,7
Lower contact	3,0	3,5	3,2	Lower contact	3,1	1,6	1,7

Appendix F: Estimation of warm bulk resistance

ΔT [°C]	L1 [$\mu\Omega$]	L2 [$\mu\Omega$]	L3 [$\mu\Omega$]	Total [$\mu\Omega$]
0	R ₀ = 218	R ₀ = 173	R ₀ = 163	R ₀ = 554
10	226,5456	179,7816	169,3896	575,7168
20	235,0912	186,5632	175,7792	597,4336
30	243,6368	193,3448	182,1688	619,1504
40	252,1824	200,1264	188,5584	640,8672
50	260,728	206,908	194,948	662,584
60	269,2736	213,6896	201,3376	684,3008
70	277,8192	220,4712	207,7272	706,0176
80	286,3648	227,2528	214,1168	727,7344
90	294,9104	234,0344	220,5064	749,4512
100	303,456	240,816	226,896	771,168
110	312,0016	247,5976	233,2856	792,8848
120	320,5472	254,3792	239,6752	814,6016

Appendix G: Steady state air temperatures and surroundings

Sensor	Position and description	Test 1		Test 2		Percentage change
		T_{abs} [°C]	ΔT [°C]	T_{abs} [°C]	ΔT [°C]	
20	Inside air Near top of compartment	60,85	38,55	56,18	34,28	11,1 %
21	Inside air Middle of compartment	47,25	24,95	42,56	20,66	17,2 %
22	Inside air Near bottom of compartment	34,92	12,62	31,05	9,15	27,5 %
	Room temperature	22,30	-	21,90		

Appendix H: Steady state temperatures of the current path

			Test 1	
			T_{abs}	ΔT
Sensor	Position and description	Module	[°C]	[°C]
Phase L1				
1	Bushing connection Cu-Cu bolted connection	Left	102,76	80,46
2	Lower switch connection Cu-Silver bolted connection	Left	116,32	94,02
3	Rotating contact	Left	116,89	94,59
4	Open/Close contact	Left	117,76	95,46
5	Upper switch connection Cu-Silver bolted connection	Left	117,94	95,64
6	Middle of busbar		113,96	91,66
7	Upper switch connection Cu-Silver bolted connection	Right	115,05	92,75
8	Open/Close contact	Right	113,93	91,63
9	Rotating contact	Right	112,77	90,47
10	Lower switch connection Cu-Silver bolted connection	Right	106,20	83,90
11	Bushing connection Cu-Cu bolted connection	Right	70,45	48,15
Phase L2				
12	Bushing connection Cu-Cu bolted connection	Left	115,90	93,60
13	Lower switch connection Cu-Silver bolted connection	Left	117,02	94,72
14	Rotating contact	Left	109,42	87,12
15	Open/Close contact	Left	115,49	93,19
16	Upper switch connection Cu-Silver bolted connection	Left	115,03	92,73
17	Middle of busbar		112,18	89,88
29	Bushing connection Cu-Cu bolted connection	Right	70,22	47,92
Phase L3				
31	Bushing connection Cu-Cu bolted connection	Left	105,34	83,04
18	Rotating contact	Left	112,93	90,63
19	Open/Close contact	Left	113,15	90,85
32	Middle of busbar		110,78	88,48
30	Bushing connection Cu-Cu bolted connection	Right	67,62	45,32

Appendices

Sensor	Position and description	Module	Test 2	
			T_{abs} [°C]	ΔT [°C]
Phase L1				
1	Bushing connection Cu-Cu bolted connection	Left	95,50	73,60
2	Lower switch connection Cu-Silver bolted connection	Left	110,70	88,80
3	Rotating contact	Left	112,36	90,46
4	Open/Close contact	Left	111,63	89,73
5	Upper switch connection Cu-Silver bolted connection	Left	112,29	90,39
6	Middle of busbar		108,37	86,47
7	Upper switch connection Cu-Silver bolted connection	Right	110,67	88,77
8	Open/Close contact	Right	110,60	88,70
9	Rotating contact	Right	110,58	88,68
10	Lower switch connection Cu-Silver bolted connection	Right	102,60	80,70
11	Bushing connection Cu-Cu bolted connection	Right	68,28	46,38
Phase L2				
12	Bushing connection Cu-Cu bolted connection	Left	107,05	85,15
13	Lower switch connection Cu-Silver bolted connection	Left	109,72	87,82
14	Rotating contact	Left	109,44	87,54
15	Open/Close contact	Left	109,20	87,30
16	Upper switch connection Cu-Silver bolted connection	Left	108,91	87,01
17	Middle of busbar		106,17	84,27
29	Bushing connection Cu-Cu bolted connection	Right	67,69	45,79
Phase L3				
31	Bushing connection Cu-Cu bolted connection	Left	98,96	77,06
18	Rotating contact	Left	106,23	84,33
19	Open/Close contact	Left	107,75	85,85
32	Middle of busbar		105,94	84,04
30	Bushing connection Cu-Cu bolted connection	Right	66,38	44,48
	Near upper switch Cu-Silver bolted connection	Right	100,70	78,80
	Near upper switch Cu-Silver bolted connection	Right	109,90	88,00

Appendix I: Calculation of heat transfer coefficient

ΔT_{con} = Average temperature on the conductor, between the measuring points [°C]

ΔT_{air} = Average temperature of the air, between the measuring points [°C]

R_0 = Resistance of the conductor under reference temperature [$\mu\Omega$]

$P_{\Delta T_{con}}$ = Resulting power loss of the part during temperature ΔT_{con} [W]

Part 1		
Temperature of the bushing	48,15	°C
Temperature of the lower switch connection	73,9	°C
ΔT_{con}	61,025	°C
Temperature of middle air	24,95	°C
Temperature of air near bottom	12,62	°C
ΔT_{air}	18,785	°C
Resulting ΔT	42,24	°C
+ Resistance from table 5.9	37,7	$\mu\Omega$
- Bulk resistance horizontal part of bar	13,65	$\mu\Omega$
= Resistance R_0	24,1	$\mu\Omega$
Resistance $R_{61,025}$	29,88	$\mu\Omega$
$P_{\Delta T_{con}}$	11,859	W
Surface area:		
Length	0,3	m
Width	0,04	m
Depth	0,006	m
Resulting surface, U	0,0276	m²
Heat transfer coefficient h	10,17	

Appendices

Part 2		
Temperature rotating contact	91,63	°C
Temperature sliding contact	90,47	°C
ΔT_{con}	91,05	°C
Temperature of air near top	38,55	°C
Temperature of middle air	24,95	°C
ΔT_{air}	31,75	°C
Resulting ΔT	59,3	°C
+Cold resistance R_0 from table 5.9	48,2	$\mu\Omega$
-Bulk resistance of "back part switch"	6,7	$\mu\Omega$
=Resistance R_0	41,5	$\mu\Omega$
Resistance R_91,05	56,35	$\mu\Omega$
$P_{\Delta T_{con}}$	22,365	W
Surface area:		
Metal plate:		
Length	0,074	m
Width	0,025	m
Resulting surface x 2	0,0037	m²
Outer side switch:		
Length	0,12	m
Width	0,022	m
Resulting surface, U	0,0053	m²
Heat transfer coefficient h	42,00	

Part 3		
ΔT_{con}	91,66	°C
ΔT_{air}	38,55	°C
Resulting ΔT	53,11	°C
Cold resistance R_0	48,8	$\mu\Omega$
Resistance R_91,05	58,99	$\mu\Omega$
$P_{\Delta T_{con}}$	23,41	W
Surface area:		
Length	0,65	m
Width	0,04	m
Resulting surface, U	0,052	m²
Heat transfer coefficient h	8,48	

Appendices

Part 4		
Temperature rotating contact	94,02	°C
Temperature sliding contact	94,59	°C
ΔT_{con}	94,305	°C
Temperature of air near top	38,55	°C
Temperature of middle air	24,95	°C
ΔT_{air}	31,75	°C
Resulting ΔT	62,555	°C
Cold resistance R_0	41,5	$\mu\Omega$
Resistance R_94,305	56,84	$\mu\Omega$
$P_{\Delta T_{con}}$	22,56	W
Surface area		
Metal plate:		
Length	0,074	m
Width	0,025	m
Resulting surface x 2	0,0037	m ²
Outer side switch		
Length	0,12	m
Width	0,022	m
Resulting surface, U	0,00528	m²
Heat transfer coefficient h	40,16	

Part 5		
Temperature of the bushing	80,46	°C
Temperature of the lower switch connection	94,02	°C
ΔT_{con}	87,24	°C
Temperature of middle air	24,95	°C
Temperature of air near bottom	12,62	°C
ΔT_{air}	18,785	°C
Resulting ΔT	68,455	°C
Cold resistance R_0	24,1	$\mu\Omega$
Resistance R_68,455	32,36	$\mu\Omega$
$P_{\Delta T_{con}}$	12,84	W
Surface area		
Length	0,3	m
Width	0,04	m
Depth	0,006	m
Resulting surface, U	0,0276	m²
Heat transfer coefficient h	6,80	